



1 **Acylperoxy radicals during ozonolysis of  $\alpha$ -pinene: composition, formation mechanism,**  
2 **and contribution to the production of highly oxygenated organic molecules**

3 Han Zang<sup>1</sup>, Dandan Huang<sup>2</sup>, Jiali Zhong<sup>3</sup>, Ziyue Li<sup>1</sup>, Chenxi Li<sup>1</sup>, Huayun Xiao<sup>1</sup>, Yue Zhao<sup>1,\*</sup>

4

5 <sup>1</sup>School of Environmental Science and Engineering, Shanghai Jiao Tong University, Shanghai,  
6 200240, China

7 <sup>2</sup>Shanghai Academy of Environmental Sciences, Shanghai 200233, China

8 <sup>3</sup>Division of Environment and Sustainability, Hong Kong University of Science and Technology,  
9 Hong Kong SAR, 999077, China

10

11 \*Correspondence: Yue Zhao (yuezhao20@sjtu.edu.cn)

12



13 **Abstract**

14 Acylperoxy radicals ( $\text{RO}_2$ ) are key intermediates in atmospheric oxidation of organic compounds  
15 and different from the general alkyl  $\text{RO}_2$  radicals in reactivity. However, direct probing of the  
16 molecular identities and chemistry of acyl  $\text{RO}_2$  remains quite limited. Here, we report a combined  
17 experimental and kinetic modelling study of the composition and formation mechanisms of acyl  
18  $\text{RO}_2$ , as well as their contributions to the formation of highly oxygenated organic molecules (HOMs)  
19 during ozonolysis of  $\alpha$ -pinene. We find that acyl  $\text{RO}_2$  radicals account for 67%, 94%, and 32% of  
20 the highly oxygenated  $\text{C}_7$ ,  $\text{C}_8$ , and  $\text{C}_9$   $\text{RO}_2$ , respectively, but only a few percent of  $\text{C}_{10}$   $\text{RO}_2$ . The  
21 formation pathway of acyl  $\text{RO}_2$  species depends on their oxygenation level. The highly oxygenated  
22 acyl  $\text{RO}_2$  (oxygen atom number  $\geq 6$ ) are mainly formed by the intramolecular aldehydic H-shift (i.e.,  
23 autoxidation) of  $\text{RO}_2$ , while the less oxygenated acyl  $\text{RO}_2$  (oxygen atom number  $< 6$ ) are basically  
24 derived from the C-C bond cleavage of alkoxy (RO) radicals containing an  $\alpha$ -ketone group or the  
25 intramolecular H-shift of RO containing an aldehyde group. The acyl  $\text{RO}_2$ -involved reactions  
26 explain 50-90% of  $\text{C}_7$  and  $\text{C}_8$  closed-shell HOMs and 14% of  $\text{C}_{10}$  HOMs, respectively. For  $\text{C}_9$  HOMs,  
27 this contribution can be up to 30%-60%. In addition, acyl  $\text{RO}_2$  contribute to 50%-95% of  $\text{C}_{14}$ - $\text{C}_{18}$   
28 HOM dimer formation. Because of the generally fast reaction kinetics of acyl  $\text{RO}_2$ , the acyl  $\text{RO}_2$  +  
29 alkyl  $\text{RO}_2$  reactions seem to outcompete the alkyl  $\text{RO}_2$  + alkyl  $\text{RO}_2$  pathways, thereby affecting the  
30 fate of alkyl  $\text{RO}_2$  and HOM formation. Our study sheds lights on the detailed formation pathways  
31 of the monoterpene-derived acyl  $\text{RO}_2$  and their contributions to HOM formation, which will help to  
32 understand the oxidation chemistry of monoterpenes and sources of low-volatility organic  
33 compounds capable of driving particle formation and growth in the atmosphere.



## 34 1. Introduction

35 Monoterpenes ( $C_{10}H_{16}$ ) comprise an important fraction of nonmethane hydrocarbons in the global  
36 atmosphere (Guenther et al., 2012; Sindelarova et al., 2014) and make a significant contribution to  
37 the secondary organic aerosol (SOA) budget (Pye et al., 2010; Iyer et al., 2021). The presence of  
38 double bond and large molecular size of monoterpenes favor their oxidation reactivity towards  $O_3$ ,  
39 hydroxyl (OH), and nitrate ( $NO_3$ ) radicals (Atkinson et al., 1990; Roger et al., 2004; Kurten et al.,  
40 2015; Kristensen et al., 2016; Bianchi et al., 2019; Berndt, 2022), as well as the formation of low-  
41 volatility products and SOA (Fry et al., 2009; Fry et al., 2014; Zhang et al., 2018; Bianchi et al.,  
42 2019; Molteni et al., 2019; Shen et al., 2022). The organic peroxy radicals ( $RO_2$ ) in the gas-phase  
43 oxidation of monoterpenes can undergo autoxidation and form a class of highly oxygenated organic  
44 compounds (HOM) (Jokinen et al., 2014; Mentel et al., 2015; Berndt et al., 2016; Zhao et al., 2018;  
45 Bianchi et al., 2019; Bell et al., 2021; Berndt, 2022), which are primarily low- or extremely low-  
46 volatility organic compounds (LVOCs and ELVOCs) (Ehn et al., 2014; Bianchi et al., 2019) and  
47 thus play a crucial role in SOA formation and growth.

48 Significant advances have been made in recent years concerning the monoterpene  $RO_2$  autoxidation  
49 and its contribution to HOM formation (Ehn et al., 2014; Berndt et al., 2016; Zhao et al., 2018; Xu  
50 et al., 2019; Lin et al., 2021; Berndt, 2022; Shen et al., 2022). It is recognized that a part of  
51 monoterpene  $RO_2$  radicals derived from the traditional ozonolysis channel (i.e., isomerization of  
52 Criegee intermediates, CI) and OH addition channel can autoxidize at a rate larger than  $1\text{ s}^{-1}$  and  
53 could be an important contributor to HOM formation (Zhao et al., 2018; Xu et al., 2019; Berndt,  
54 2021). Recently, new reaction channels leading to the  $RO_2$  radicals that can undergo fast  
55 autoxidation have been proposed. A quantum chemical calculation study indicated that an excited  
56 CI arising from  $\alpha$ -pinene ozonolysis could undergo ring-breaking reactions and directly lead to a  
57 ring-opened  $RO_2$  due to the excess energy, which can autoxidize at a rate of  $\sim 1\text{ s}^{-1}$  and rapidly form  
58 highly oxidized  $RO_2$  with up to 8 oxygen atoms (Iyer et al., 2021). In addition, the minor hydrogen  
59 abstraction channel by OH radicals has been proposed as a predominant pathway to HOM formation  
60 from OH oxidation of  $\alpha$ -pinene under atmospheric conditions (Shen et al., 2022).

61  $RO_2$  species can be simply divided into alkyl  $RO_2$  and acyl  $RO_2$  ( $RC(O)OO$ ) according to whether  
62 R is an acyl radical. There are significant differences in the reactivity of these two kinds of  $RO_2$ .  
63 Firstly, the rate constant of acyl  $RO_2$  with NO is in general slightly higher than that of alkyl  $RO_2$   
64 (Atkinson et al., 2007; Calvert et al., 2008; Orlando and Tyndall, 2012). For example, the reaction  
65 rate constants of acyl  $RO_2$ ,  $CH_3C(O)O_2$ , and alkyl  $RO_2$ ,  $CH_3CH_2O_2$ , with NO have been reported to  
66 be  $20 \times 10^{-12}\text{ cm}^3\text{ molecule}^{-1}\text{ s}^{-1}$  and  $9.2 \times 10^{-12}\text{ cm}^3\text{ molecule}^{-1}\text{ s}^{-1}$ , respectively (Atkinson et al., 2007;



67 Calvert et al., 2008; Orlando and Tyndall, 2012). Besides, acyl RO<sub>2</sub> can react rapidly with NO<sub>2</sub> and  
68 form thermally unstable peroxyacyl nitrates (RC(O)OONO<sub>2</sub>), which have a lifetime of tens of  
69 minutes at room temperature and of days and even months in winter or in the upper atmosphere with  
70 lower temperatures (Atkinson et al., 2007; Orlando and Tyndall, 2012). Although alkyl RO<sub>2</sub> radicals  
71 can also react with NO<sub>2</sub> and form the alkyl peroxy nitrates (ROONO<sub>2</sub>), they are extremely unstable  
72 and will decompose into RO<sub>2</sub> radicals and NO<sub>2</sub> in less than 1s (Kirchner et al., 1997; Orlando and  
73 Tyndall, 2012). Lastly, the rate constant of cross-reaction of acyl RO<sub>2</sub> ( $1.5 \pm 0.3 \times 10^{-11}$  cm<sup>3</sup>  
74 molecule<sup>-1</sup> s<sup>-1</sup>) is significantly higher than that of alkyl RO<sub>2</sub> ( $2 \times 10^{-17}$  -  $1 \times 10^{-11}$  cm<sup>3</sup> molecule<sup>-1</sup> s<sup>-1</sup>)  
75 (Villenave and Lesclaux, 1996; Tyndall et al., 2001; Atkinson et al., 2007; Zhao et al., 2018). As a  
76 result, these two kinds of RO<sub>2</sub> may play different roles in the autoxidation as well as HOM and  
77 dimer formation.

78 The quantum calculations revealed that different functional groups in RO<sub>2</sub> would lead to  
79 significantly different intramolecular H-shift rates (Otkjær et al., 2018). The C=O and C=C  
80 substituents lead to resonance stabilized carbon radicals and could enhance the H-shift rate constants  
81 by more than a factor of 400. The fast aldehydic H-shift rate contributes to a series of acyl radicals  
82 (RC(O)) with the radical site at the terminal carbonyl carbon, which further produce the acyl RO<sub>2</sub>  
83 with O<sub>2</sub> addition. Many RO<sub>2</sub> formed in the oxidation of monoterpenes have the aldehyde  
84 functionality, especially for  $\alpha$ -pinene ozonolysis, in which all the primary and many later-generation  
85 RO<sub>2</sub> contain at least one aldehyde group (Nozriere et al., 2015; Berndt et al., 2018; Li et al., 2019;  
86 Berndt, 2022; Zhao et al., 2022). As a result, acyl RO<sub>2</sub> may comprise a considerable fraction of total  
87 RO<sub>2</sub> species and contribute significantly to the formation of low-volatility products and SOA in the  
88 monoterpene oxidation system. A recent study by Zhao et al. (2022) found that the acyl RO<sub>2</sub>-  
89 involved reactions contribute to 50%-80% of oxygenated C<sub>15</sub>-C<sub>20</sub> dimers (O:C  $\geq$  0.4) and 70% of  
90 C<sub>15</sub>-C<sub>19</sub> dimer esters in SOA from  $\alpha$ -pinene ozonolysis. However, currently the direct probing of  
91 the molecular identities and chemistry of monoterpene-derived acyl RO<sub>2</sub> radicals is rather limited.  
92 The role of acyl RO<sub>2</sub> in HOM formation remains to be quantified.

93 In this study, the molecular identities and formation mechanisms of acyl RO<sub>2</sub> radicals, as well as  
94 their contributions to HOM formation in the  $\alpha$ -pinene ozonolysis are investigated. The experiments  
95 were conducted in a flow reactor with different concentrations of NO<sub>2</sub>, which acted as an efficient  
96 scavenger for the acyl RO<sub>2</sub>. The molecular composition and abundance of the gas-phase HOMs  
97 were measured by a chemical ionization-atmospheric pressure interface-time-of-flight mass  
98 spectrometer (CI-API-TOF) using nitrate as the reagent ions. In addition, kinetic modelling using  
99 the Framework for 0-D Atmospheric Modeling (F0AM v4.1) employing Master Chemical



100 Mechanisms (MCM v3.3.1) updated with the latest advances of the RO<sub>2</sub> chemistry was performed  
101 to gain insights into the reaction kinetics and mechanisms of acyl RO<sub>2</sub> species. We find that acyl  
102 RO<sub>2</sub> account for a major fraction of highly oxygenated C<sub>7</sub> and C<sub>8</sub> RO<sub>2</sub> and play a significant role in  
103 the formation of HOM monomers and dimers with small molecular size. This study will help to  
104 understand the role of acyl RO<sub>2</sub> in the formation of low-volatility species from monoterpene  
105 oxidation and reduce the uncertainties in the future atmospheric modelling of the formation and  
106 impacts of aerosols.

## 107 2. Method and Materials

### 108 2.1 Flow Reactor Experiments.

109 The  $\alpha$ -pinene ozonolysis experiments were carried out under room temperature (298 K) and dry  
110 conditions (relative humidity < 5%) in a custom-built flow reactor, which has been described in detail  
111 previously (Yao et al., 2019). The  $\alpha$ -pinene vapor was generated by evaporating its pure liquid (99%,  
112 Sigma-Aldrich) into a flow of zero air (10.65 L min<sup>-1</sup>) added to the reactor using an automated  
113 syringe pump (TYD01-01-CE, Baoding Leifu Fluid Technology Co., Ltd.). The initial  
114 concentrations of  $\alpha$ -pinene ranged from 500 ppb to 3 ppm in different experiments. Ozone was  
115 generated by passing a flow of ultra-high-purity (UHP) O<sub>2</sub> (150 mL min<sup>-1</sup>, Shanghai Maytor Special  
116 Gas Co., Ltd.) through a quartz tube housing a pen-ray mercury lamp (UV-S2, UVP Inc.) and its  
117 concentration (45 ppb and 180 ppb under low and high O<sub>3</sub> conditions, respectively) was measured  
118 by an ozone analyzer (Model 49i, Thermo Fisher Scientific, USA). The NO<sub>2</sub>, acting as an acyl RO<sub>2</sub>  
119 scavenger, was derived from its standard cylinder gas (15.6 ppm, Shanghai Weichuang Standard  
120 Gas Co., Ltd.) and its initial concentration ranged from 0 to 30 ppb. To validate the formation  
121 mechanisms of acyl RO<sub>2</sub>, selected experiments with the addition of NO or cyclohexane were also  
122 conducted. NO was derived by its standard cylinder gas (9.8 ppm, Shanghai Weichuang Standard  
123 Gas Co., Ltd.) and its initial concentration also ranged from 0 to 30 ppb. The gas-phase cyclohexane  
124 (~ 500 ppm), acting as an OH scavenger, was generated by bubbling a gentle flow of UHP N<sub>2</sub>  
125 through liquid cyclohexane (LC-MS grade, CNW). The total air flow in the flow reactor was 10.8 L  
126 min<sup>-1</sup> and the residence time was 25 seconds. The relatively low O<sub>3</sub> concentration and short reaction  
127 time in the flow reactor avoid significant production of NO<sub>3</sub> radicals from NO<sub>2</sub> and O<sub>3</sub> and make  
128 the NO<sub>3</sub> oxidation contribute only 0.3%-1.2% of the total  $\alpha$ -pinene oxidation in our experiments.  
129 Therefore, the NO<sub>3</sub> chemistry could be neglected in this study. A summary of the experimental  
130 conditions is given in Tables S1 and S2 in the Supplement.

131 The gas-phase RO<sub>2</sub> radicals and closed-shell products were measured by a nitrate-based CI-API-  
132 TOF mass spectrometer (abbreviated as nitrate-CIMS; Aerodyne Research, Inc.), and a long time-



133 of-flight mass spectrometer with a mass resolution of  $\sim 10000$  Th/Th was used here. The mass  
134 calibration error is below 1.8 ppm. The sheath flow, including a  $2 \text{ mL min}^{-1}$  UHP  $\text{N}_2$  flow containing  
135 nitric acid ( $\text{HNO}_3$ ) and  $22.4 \text{ L min}^{-1}$  zero air was guided through a PhotoIonizer X-ray (Model L9491,  
136 Hamamatsu, Japan) to generate nitrate reagent ions. The total sample flow rate was  $9 \text{ L min}^{-1}$  during  
137 the experiments. The instrument was calibrated with a sulfuric acid ( $\text{H}_2\text{SO}_4$ ) calibration factor and  
138 a mass-dependent transmission efficiency. The mass spectra within the  $m/z$  range of 50 to 700 were  
139 analyzed using the tofTools package developed by Junninen et al. (2010) based on Matlab. After  
140 getting the signals of the gas-phase oxygenated organic molecules (OOMs), their concentration can  
141 be calculated as follows (Jokinen et al., 2012; Bianchi et al., 2019):

$$142 \quad [\text{OOM}] = C \times \frac{I_{\text{OOM}}}{I_{\text{NO}_3^-} + I_{\text{HNO}_3\text{NO}_3^-} + I_{\text{HNO}_3\text{HNO}_3\text{NO}_3^-}} \times \frac{1}{T_i} \quad (1)$$

143  $C$  is the calibration factor of  $\text{H}_2\text{SO}_4$ , with a value of  $4.06 \times 10^9$  molecule  $\text{cm}^{-3}$  in this study;  $I_X$  is the  
144 detected signal of  $X$  in the unit of counts per second (cps) and most OOMs were detected as adducts  
145 with  $\text{NO}_3^-$ ;  $T_i$  is the mass-dependent transmission efficiency of the instrument determined using the  
146 following equation by adding propanoic acid, pentanoic acid and heptanoic acid vapors to deplete  
147  $\text{NO}_3^-$  (Figure S1):

$$148 \quad T_i = 0.56 + 7.2 \times 10^4 / ((m/z - 498.84)^2 + 3.46 \times 10^4) \quad (2)$$

## 149 2.2 Kinetic Model Simulations.

150 Model simulations of  $\text{RO}_2$  and HOM formation in selected experiments were performed to constrain  
151 the reaction kinetics and mechanisms of acyl  $\text{RO}_2$  using FOAM v4.1 (Wolfe et al., 2016), which  
152 employs MCM v3.3.1 (Jenkin et al., 2015) updated with the chemistry of  $\text{RO}_2$  autoxidation and  
153 cross-reactions forming HOM monomers and dimers. Newly added species and reactions to MCM  
154 v3.3.1 followed the work by Zhao et al. (2018) and Wang et al. (2021). Considering that the default  
155 MCM v3.3.1 does not include highly oxygenated acyl  $\text{RO}_2$ , we added the possible formation  
156 pathways of the potential acyl  $\text{RO}_2$  measured in this study to the model based on the mechanisms  
157 proposed by Zhao et al. (2022).

158 The formation and reaction branching ratios of the two  $\alpha$ -pinene-derived CIs are updated in the  
159 model according to the recent studies (Table S3) (Claflin et al., 2018; Iyer et al., 2021; Zhao et al.,  
160 2021; Berndt, 2022). The formation of a ring-opened  $\text{C}_{10}\text{H}_{15}\text{O}_4\text{-RO}_2$  species ( $\text{C}_{10}\text{H}_{15}\text{O}_4\text{RBRO}_2$  in  
161 Table S3) from  $\alpha$ -pinene ozonolysis proposed by a recent study (Iyer et al., 2021), as well as its  
162 subsequent autoxidation and bimolecular reactions, is included in the model. The autoxidation rate  
163 constant of the ring-opened  $\text{C}_{10}\text{H}_{15}\text{O}_4\text{-RO}_2$  is  $1 \text{ s}^{-1}$ , and a lower limit of its molar yield (30%) was



164 used according to the recent studies (Zhao et al., 2021; Meder et al., 2023) and our results (see  
165 details in Section 3.3). We also added the hydrogen abstraction channel of  $\alpha$ -pinene oxidation by  
166 OH radicals according to a recent study (Shen et al., 2022). The branching ratio of this channel was  
167 set to 9%, with the rest 91% being the traditional OH addition pathways. The detailed reaction  
168 pathways and rate constants of RO<sub>2</sub> species in this channel followed the work by Shen et al. (2022),  
169 except for RO<sub>2</sub> cross-reactions, the rates of which were not reported in that study. As the primary  
170 RO<sub>2</sub> radicals (C<sub>10</sub>H<sub>15</sub>O<sub>2</sub>-RO<sub>2</sub>) formed via the hydrogen abstraction by OH radical are least-oxidized  
171 with only 2 oxygen atoms, their cross-reaction rate could be relatively low (Atkinson et al., 2007;  
172 Orlando and Tyndall, 2012). In the model, this rate constant was set to  $1 \times 10^{-13}$  cm<sup>3</sup> molecule<sup>-1</sup> s<sup>-1</sup>.  
173 For other alkyl RO<sub>2</sub> radicals (including HOM-RO<sub>2</sub>), their cross-reaction rate constant is assumed to  
174 be  $1 \times 10^{-12}$  cm<sup>3</sup> molecule<sup>-1</sup> s<sup>-1</sup> according to Zhao et al. (2018). The dimer formation rates for these  
175 alkyl RO<sub>2</sub> are same as their cross-reaction rates.

176 In flow reactor experiments, the equilibrium formation of ROONO<sub>2</sub> would lead to the consumption  
177 of alkyl RO<sub>2</sub> radicals. To account for the influence of this process on the RO<sub>2</sub> budget and HOM  
178 formation, we included the reaction of RO<sub>2</sub> + NO<sub>2</sub>  $\rightleftharpoons$  ROONO<sub>2</sub> in the model, with forward and  
179 reverse reaction rate constants of  $7.5 \times 10^{-12}$  cm<sup>3</sup> molecule<sup>-1</sup> s<sup>-1</sup> and 5 s<sup>-1</sup>, respectively (Orlando and  
180 Tyndall, 2012). To simplify the parameterization, the forward and reverse reaction rate constants of  
181 newly added highly oxygenated acyl RO<sub>2</sub> with NO<sub>2</sub> are the same as default values in MCM v3.3.1.  
182 Besides, the cross-reaction rate constants of acyl RO<sub>2</sub> (including acyl RO<sub>2</sub> + acyl RO<sub>2</sub> and acyl RO<sub>2</sub>  
183 + alkyl RO<sub>2</sub>) forming monomers or dimers were both set to  $1 \times 10^{-11}$  cm<sup>3</sup> molecule<sup>-1</sup> s<sup>-1</sup> (Orlando  
184 and Tyndall, 2012). Considering that there are large uncertainties in the dimer formation rate of RO<sub>2</sub>,  
185 a sensitivity analysis was conducted to evaluate its influence on acyl RO<sub>2</sub>-involved HOM formation  
186 by varying the rate constant from  $1 \times 10^{-13}$  cm<sup>3</sup> molecule<sup>-1</sup> s<sup>-1</sup> to  $1 \times 10^{-12}$  cm<sup>3</sup> molecule<sup>-1</sup> s<sup>-1</sup> for alkyl  
187 RO<sub>2</sub> and  $1 \times 10^{-12}$  cm<sup>3</sup> molecule<sup>-1</sup> s<sup>-1</sup> to  $1 \times 10^{-11}$  cm<sup>3</sup> molecule<sup>-1</sup> s<sup>-1</sup> for acyl RO<sub>2</sub>. The results show that  
188 changes in dimer formation rate constants within the above ranges have no significant influence on  
189 the contribution of acyl RO<sub>2</sub> to HOM formation (Figure S2).

190 The wall losses of OH, HO<sub>2</sub>, and RO<sub>2</sub> radicals, as well as closed-shell HOM monomers and dimers  
191 in the flow reactor were considered using the KPS method proposed by Knopf et al. (2015) in the  
192 model (Table S4), with an assumption of irreversible uptake of these species on the reactor wall. It  
193 is found that the wall loss of OH, HO<sub>2</sub>, and RO<sub>2</sub> radicals accounts for 0.08-0.14%, 4.7-9.1%, and 7.3-  
194 25.5% of their total production, respectively, with lower values under higher reacted  $\alpha$ -pinene  
195 concentration conditions. Therefore, the wall loss process would not significantly influence  $\alpha$ -  
196 pinene oxidation and RO<sub>2</sub> chemistry. The wall losses of closed-shell HOM monomers and dimers

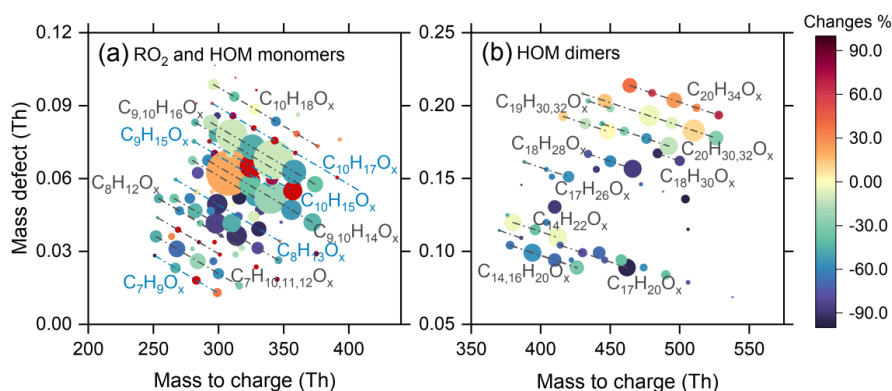


197 account for 18.4-34.7% and 14.2-33.1% of their total production, respectively. It should be noted  
 198 that the wall losses of typical RO<sub>2</sub> and HOMs have negligible impact on their responses to the  
 199 addition of NO<sub>2</sub> (Figure S3). In addition, with the consideration of the wall loss effects, the effect  
 200 and contribution of acyl RO<sub>2</sub> to the HOM formation only changed a little (0.02-0.5%). Therefore,  
 201 the wall losses of RO<sub>2</sub> and HOMs in the flow reactor would not affect the interpretation of the results  
 202 in this study.

### 203 3. Results and Discussion

#### 204 3.1 Molecular composition of acyl RO<sub>2</sub> from $\alpha$ -pinene ozonolysis

205 The overall formation characteristics of gas-phase RO<sub>2</sub>, closed-shell monomers, and dimers with  
 206 the addition of NO<sub>2</sub> (30 ppb) is shown in Figure 1 (Exps 8 and 14, Table S1). Since nitrate-CIMS is  
 207 only highly sensitive to the highly oxygenated species, we only discuss the production of HOMs  
 208 with oxygen atoms above 6 here. As for RO<sub>2</sub> and closed-shell monomers (Figure 1a), the  
 209 concentrations of C<sub>7</sub> and C<sub>8</sub> species decrease by more than 50% with the addition of NO<sub>2</sub>, while for  
 210 C<sub>9</sub> and C<sub>10</sub> species, their decreases are relatively small (within 40%). In addition, we note that there  
 211 is an unexpected increase in some C<sub>9</sub> and C<sub>10</sub> RO<sub>2</sub>, and the possible reason will be discussed in  
 212 detail in Section 3.3.



213  
 214 Figure 1 Mass defect plots of (a) RO<sub>2</sub>, HOM monomers, and (b) HOM dimers formed from  
 215 ozonolysis of  $\alpha$ -pinene in the presence of NO<sub>2</sub> measured using nitrate-CIMS (Exps 8, 14). The  
 216 circles are colored by the relative changes in concentration of RO<sub>2</sub>, monomers and dimers due to  
 217 the addition of NO<sub>2</sub> (30 ppb). The area of circles is linearly scaled with the cube root of the  
 218 concentration of HOMs formed in the absence of NO<sub>2</sub>. The blue lines represent RO<sub>2</sub> radicals.

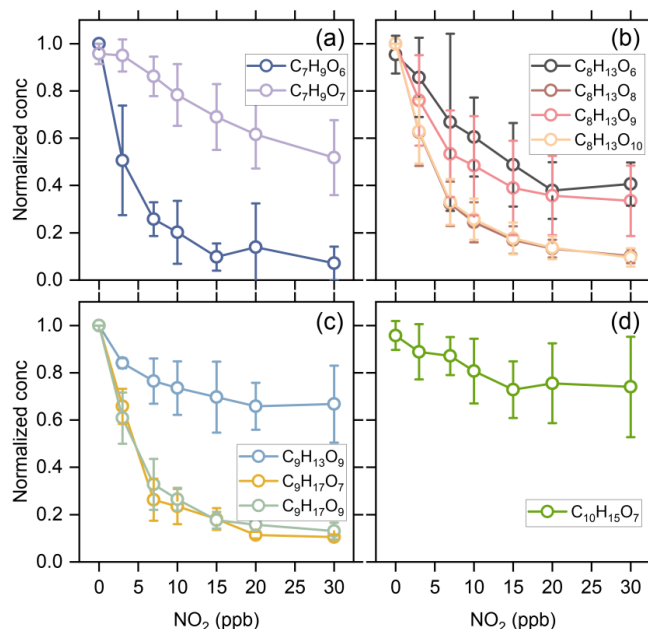
219 NO<sub>2</sub> could react rapidly with acyl RO<sub>2</sub> radicals to form RC(O)OONO<sub>2</sub>, which has a higher thermal-  
 220 stability compared to ROONO<sub>2</sub> and can serve as a sink for acyl RO<sub>2</sub> on our experimental timescales.





221 Therefore, a significant decrease in C<sub>7</sub> and C<sub>8</sub> RO<sub>2</sub> and HOMs upon the addition of NO<sub>2</sub> indicates  
222 that a major fraction of C<sub>7</sub> and C<sub>8</sub> RO<sub>2</sub> are acyl RO<sub>2</sub>. In contrast, the slight decrease in C<sub>9</sub> and C<sub>10</sub>  
223 HOM monomers shows that the contribution of acyl RO<sub>2</sub> to C<sub>9</sub> and C<sub>10</sub> RO<sub>2</sub> is relatively small.  
224 However, some of the C<sub>10</sub> monomers showed a slight increase with the addition of NO<sub>2</sub>, especially  
225 for C<sub>10</sub>H<sub>18</sub>O<sub>x</sub>-HOMs. The addition of NO<sub>2</sub> plays a twofold role in dimer formation from  $\alpha$ -pinene  
226 ozonolysis (Figure 1b). There is a significant inhibiting effect on C<sub>14</sub>-C<sub>18</sub> dimers, which is due to  
227 the large contribution of acyl RO<sub>2</sub> to the total C<sub>7</sub> and C<sub>8</sub> RO<sub>2</sub> that generate such dimers. However,  
228 C<sub>19</sub> and C<sub>20</sub> dimers only show a slight decrease with the addition of NO<sub>2</sub>, and some of them are even  
229 enhanced. In particular, the enhancement in C<sub>20</sub>H<sub>34</sub>O<sub>x</sub> is most significant, reaching 30%.

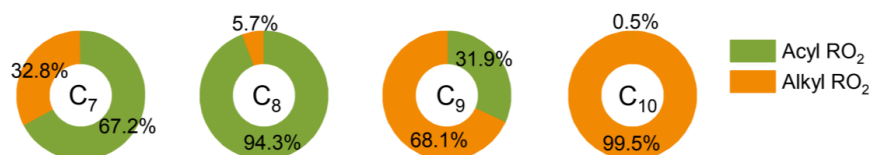
230 Kinetic model simulations show that the concentration of alkyl RO<sub>2</sub> decreases by 1-20% with the  
231 addition of 30 ppb NO<sub>2</sub> under different reacted  $\alpha$ -pinene conditions (Exps 1-28). Considering that  
232 the acyl RO<sub>2</sub> could be rapidly consumed by NO<sub>2</sub>, if the concentration reduction of a RO<sub>2</sub> species  
233 significantly exceeds 20% with 30 ppb NO<sub>2</sub> addition, we presume it has significant contribution  
234 from acyl RO<sub>2</sub>. As a result, a total of 10 acyl RO<sub>2</sub> were identified according to the changes of RO<sub>2</sub>  
235 concentration as a function of initial NO<sub>2</sub> concentration, which include C<sub>7</sub>H<sub>9</sub>O<sub>6</sub>, C<sub>7</sub>H<sub>9</sub>O<sub>7</sub>, C<sub>8</sub>H<sub>13</sub>O<sub>6</sub>,  
236 C<sub>8</sub>H<sub>13</sub>O<sub>8</sub>, C<sub>8</sub>H<sub>13</sub>O<sub>9</sub>, C<sub>8</sub>H<sub>13</sub>O<sub>10</sub>, C<sub>9</sub>H<sub>15</sub>O<sub>9</sub>, C<sub>9</sub>H<sub>17</sub>O<sub>7</sub>, C<sub>9</sub>H<sub>17</sub>O<sub>9</sub>, and C<sub>10</sub>H<sub>15</sub>O<sub>7</sub>. Figure 2 shows the  
237 averaged normalized acyl RO<sub>2</sub> concentrations measured as a function of the added NO<sub>2</sub>  
238 concentration under different experimental conditions (Exps 1-28). Similarly, since nitrate-CIMS is  
239 only highly sensitive to products with high oxygen content, we only observed acyl RO<sub>2</sub> with oxygen  
240 atoms above 6. Consistent with the significant decrease in C<sub>7</sub> and C<sub>8</sub> species with the addition of  
241 NO<sub>2</sub> in Figure 1a, C<sub>7</sub> and C<sub>8</sub> acyl RO<sub>2</sub> decrease by more than 50% with the increase of NO<sub>2</sub>  
242 concentration (Figures 2a, b). For C<sub>9</sub> acyl RO<sub>2</sub>, the C<sub>9</sub>H<sub>17</sub>O<sub>7</sub>-RO<sub>2</sub> and C<sub>9</sub>H<sub>17</sub>O<sub>9</sub>-RO<sub>2</sub> also decrease  
243 dramatically with increasing NO<sub>2</sub>, and the decrease in C<sub>9</sub>H<sub>13</sub>O<sub>9</sub>-RO<sub>2</sub> is relatively smaller (Figure  
244 2c). In addition, C<sub>10</sub>H<sub>15</sub>O<sub>7</sub>-RO<sub>2</sub> also shows a small decrease (Figure 2d), with a reduction of only  
245 30% at 30 ppb NO<sub>2</sub>. The relative small reduction in the abundance of some of these RO<sub>2</sub> radicals  
246 indicates the presence of alkyl RO<sub>2</sub> radicals with the same chemical formulas.



247

248 Figure 2 Averaged normalized concentration of the measured acyl RO<sub>2</sub> as a function of the added  
 249 NO<sub>2</sub> concentration under different experimental conditions (Exps 1-28).

250 Figure 3 shows the contribution of acyl and alkyl RO<sub>2</sub> to the highly oxidized C<sub>7</sub>-C<sub>10</sub> RO<sub>2</sub>. Acyl RO<sub>2</sub>  
 251 contribute 67.2%, 94.3% and 31.9% to the total C<sub>7</sub>, C<sub>8</sub>, and C<sub>9</sub> RO<sub>2</sub> concentrations, respectively. By  
 252 contrast, the only C<sub>10</sub> acyl RO<sub>2</sub> measured in this study is C<sub>10</sub>H<sub>15</sub>O<sub>7</sub>, which contributes to only 0.5%  
 253 of the total C<sub>10</sub> RO<sub>2</sub>. It should be note that there might be other C<sub>10</sub> acyl RO<sub>2</sub> that were not observed  
 254 due to the interferences from the alkyl RO<sub>2</sub> with the same chemical formulas, which respond  
 255 differently to the addition of NO<sub>2</sub> than acyl RO<sub>2</sub> do (see details in the following discussion).  
 256 Considering that some RO<sub>2</sub> formulas such as C<sub>10</sub>H<sub>15</sub>O<sub>7</sub> may have contributions from both acyl RO<sub>2</sub>  
 257 and alkyl RO<sub>2</sub>, we assumed the decrease of RO<sub>2</sub> concentration with the addition of NO<sub>2</sub> as the  
 258 concentration of acyl RO<sub>2</sub>. Besides, it is obvious that the normalized concentration basically  
 259 decreases to the lowest value when the initial NO<sub>2</sub> concentration reaches 10 ppb (Figure 2),  
 260 indicating that most of the acyl RO<sub>2</sub> are depleted at this NO<sub>2</sub> concentration. In addition, the  
 261 decreasing extents of some acyl RO<sub>2</sub> are different for different reacted α-pinene concentrations, with  
 262 lower decreasing extent for higher reacted α-pinene concentrations (Figure S4). This difference  
 263 might be due to the promoted cross-reactions of acyl RO<sub>2</sub> as well as their precursor RO<sub>2</sub> at higher  
 264 α-pinene concentrations, which are competitive with the reactions leading to acyl RO<sub>2</sub> formation as  
 265 well as the acyl RO<sub>2</sub> + NO<sub>2</sub> reactions.



266  
267 Figure 3 Contributions of acyl and alkyl RO<sub>2</sub> to the highly oxygenated C<sub>7</sub>-C<sub>10</sub> RO<sub>2</sub> measured by  
268 nitrate-CIMS.

269 In addition to the changes of acyl RO<sub>2</sub> concentration, we also show the changes of normalized alkyl  
270 RO<sub>2</sub> concentration with the increasing initial NO<sub>2</sub> concentration in Figure S5. Although ROONO<sub>2</sub>  
271 formed by the reaction of alkyl RO<sub>2</sub> with NO<sub>2</sub> is thermally unstable and would decompose quickly  
272 to release RO<sub>2</sub>, it would still reach a formation/decomposition equilibrium in the system, thus  
273 consuming a small amount of alkyl RO<sub>2</sub>. However, it can be seen from Figure S5 that during 25 s  
274 of reaction in the flow reactor, a large part of alkyl RO<sub>2</sub> has an increasing trend with the increase of  
275 NO<sub>2</sub> concentration. We speculate that a portion of ROONO<sub>2</sub> could decompose back to RO<sub>2</sub> and NO<sub>2</sub>  
276 in the nitrate-CI inlet where the sample gases were diluted instantly and the equilibrium of ROONO<sub>2</sub>  
277 was disturbed, resulting in the release of a large amount of RO<sub>2</sub>.

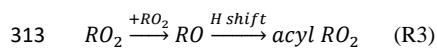
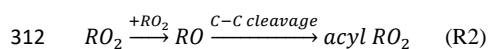
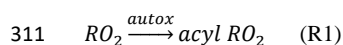
278  
279 To verify our speculation, the decomposition of ROONO<sub>2</sub> in the CI inlet was simulated based on  
280 the dilution ratio (1:3.5) and residence time (200 ms) in the inlet. As shown in Figure S6, more than  
281 40% of ROONO<sub>2</sub> decompose back to RO<sub>2</sub> and NO<sub>2</sub> in the CI inlet, which would inevitably lead to  
282 an increase in RO<sub>2</sub> concentration. As the C<sub>10</sub>H<sub>15</sub>O<sub>8</sub>NO<sub>2</sub> has a significant contribution from the  
283 relative stable RC(O)OONO<sub>2</sub> arising from the ring-opened acyl C<sub>10</sub>H<sub>15</sub>O<sub>8</sub>-RO<sub>2</sub> reported by Iyer et  
284 al. (2021), its decomposition is relatively small (~21%). It should be noted that the RO<sub>2</sub> measured  
285 here is only a part of total RO<sub>2</sub> and that a large amount of RO<sub>2</sub> has already reacted to form closed-  
286 shell products as well as ROONO<sub>2</sub> in the flow reactor. Taking Exp 14 as an example (30 ppb NO<sub>2</sub>),  
287 the simulated concentrations of RO<sub>2</sub> and ROONO<sub>2</sub> are 1.3 ppb and 1.9 ppb, which approximately  
288 accounts for 27.1% and 39.6% of the total production of RO<sub>2</sub>, respectively. Therefore, the  
289 decomposition of ROONO<sub>2</sub> could indeed result in an increase in the RO<sub>2</sub> concentration. It should  
290 also be pointed out that because of the very short residence time in the CI inlet, such an increase in  
291 the RO<sub>2</sub> concentration would not significantly impact HOM formation.

292 To confirm the reliability of our results, we examined the changes in the concentrations of RO<sub>2</sub> and  
293 closed-shell products as a function of reacted α-pinene in the absence of NO<sub>2</sub> (Section S1 and Figure  
294 S7), and the results are consistent with previous studies (Zhao et al., 2018). In addition, we repeated  
295 Exps 15-21 on another nitrate-CIMS and a similar increase in alkyl RO<sub>2</sub> signals with the addition  
296 of NO<sub>2</sub> was observed on that instrument (Figure S8).



297 **3.2 Formation mechanisms of acyl RO<sub>2</sub> during α-pinene ozonolysis**

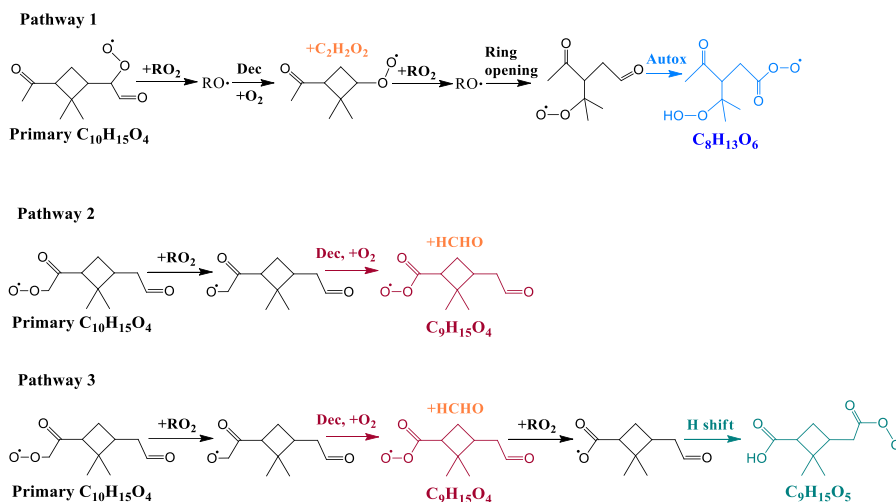
298 It has been recently suggested that there are three main pathways that directly lead to the formation  
299 of monoterpene-derived acyl RO<sub>2</sub> (Zhao et al., 2022): (i) the autoxidation of RO<sub>2</sub> containing  
300 aldehyde groups (Reaction R1), (ii) the cleavage of C-C bond of RO containing an α-ketone group  
301 (Reaction R2), and (iii) the intramolecular H-shift of RO containing an aldehyde group (Reaction  
302 R3). Here, we further investigated the formation mechanisms of acyl RO<sub>2</sub>. Figure 4 shows the  
303 reaction schemes leading to the formation of example acyl RO<sub>2</sub> radicals. The detailed formation  
304 mechanisms of acyl RO<sub>2</sub> measured in this study are shown in Figure S9. The formation of acyl RO<sub>2</sub>,  
305 especially those having the small molecular size (C<sub>7</sub>-C<sub>9</sub>), requires the production and subsequent  
306 decomposition (or ring-opening process) of RO radicals. Take C<sub>8</sub>H<sub>13</sub>O<sub>6</sub>-RO<sub>2</sub> as an example (Figure  
307 4), two steps of RO formation and decomposition following the primary C<sub>10</sub>H<sub>15</sub>O<sub>4</sub>-RO<sub>2</sub> lead to the  
308 ring-opened C<sub>8</sub>H<sub>13</sub>O<sub>4</sub>-RO<sub>2</sub> that can undergo rapid aldehydic H-shift to form the acyl RO<sub>2</sub>. While for  
309 C<sub>8</sub>H<sub>13</sub>O<sub>9</sub>-RO<sub>2</sub>, it directly comes from the aldehydic H-shift of C<sub>8</sub>H<sub>13</sub>O<sub>7</sub>-RO followed by the O<sub>2</sub>  
310 addition (Figure S9).



314



315



316

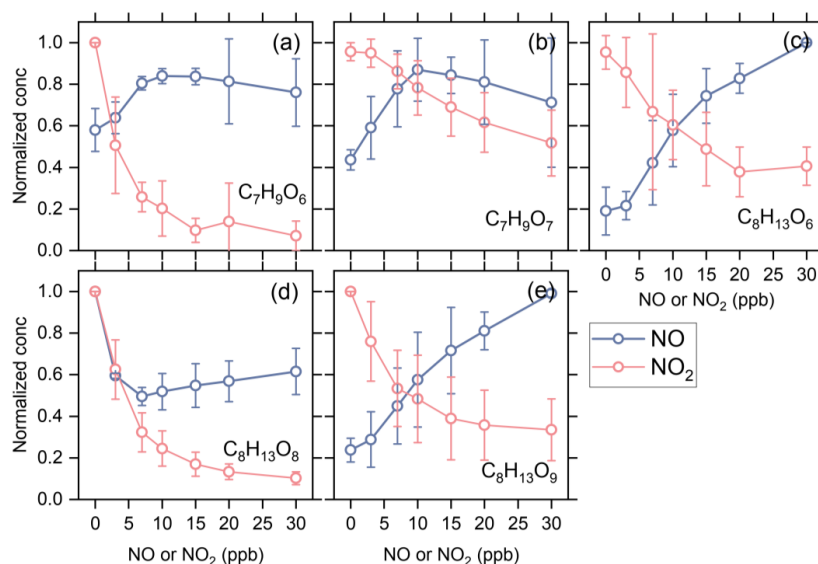
317

318 Figure 4 Three different formation pathways of acyl RO<sub>2</sub> during ozonolysis of  $\alpha$ -pinene. The acyl  
 319 RO<sub>2</sub>, C<sub>9</sub>H<sub>15</sub>O<sub>4</sub> and C<sub>9</sub>H<sub>15</sub>O<sub>5</sub>, formed via pathways 2 and 3, respectively, were not detected by nitrate-  
 320 CIMS in this study due to their relatively low oxygenation level.

321 To verify the formation mechanisms of acyl RO<sub>2</sub>, we added NO in some experiments (Exps 33-56)  
 322 to see how acyl RO<sub>2</sub> respond to the increasing NO concentration. As shown in Figure 5, the changes  
 323 of C<sub>7</sub> and C<sub>8</sub> acyl RO<sub>2</sub> show opposite trend with the increasing NO and NO<sub>2</sub> concentration, except  
 324 for C<sub>8</sub>H<sub>13</sub>O<sub>8</sub>-RO<sub>2</sub>. NO can react with RO<sub>2</sub> to form RO radicals and promote the formation of RO<sub>2</sub>  
 325 that requires the involvement of RO radicals in their formation. In addition to C<sub>8</sub>H<sub>13</sub>O<sub>6</sub>-RO<sub>2</sub>  
 326 discussed above, the formation of C<sub>7</sub>H<sub>9</sub>O<sub>7</sub>-RO<sub>2</sub> and C<sub>8</sub>H<sub>13</sub>O<sub>9</sub>-RO<sub>2</sub> needs 2 and 4 steps of the RO  
 327 formation following C<sub>10</sub>H<sub>15</sub>O<sub>4</sub>-RO<sub>2</sub> (Figure S9), respectively. Therefore, the increase of RO  
 328 concentration due to the addition of NO would promote the production of these acyl RO<sub>2</sub>. These  
 329 results prove that the RO radicals indeed play an important role in the acyl RO<sub>2</sub> formation. While  
 330 for C<sub>8</sub>H<sub>13</sub>O<sub>8</sub>-RO<sub>2</sub>, its concentration decreases substantially with the addition of NO up to 3 ppb,  
 331 similar to the trend observed with the addition of NO<sub>2</sub>. After reaching the minimum at 7 ppb NO,  
 332 the concentration of C<sub>8</sub>H<sub>13</sub>O<sub>8</sub>-RO<sub>2</sub> tends to increase with the further increase of NO concentration.  
 333 Given that C<sub>8</sub>H<sub>13</sub>O<sub>8</sub>-RO<sub>2</sub> is likely to directly come from the autoxidation of C<sub>8</sub>H<sub>13</sub>O<sub>6</sub> acyl RO<sub>2</sub> (see  
 334 Figure S9), the rapid consumption of C<sub>8</sub>H<sub>13</sub>O<sub>6</sub>-RO<sub>2</sub> by NO and NO<sub>2</sub> (formed by O<sub>3</sub> oxidation of NO)  
 335 may outcompete its autoxidation process, thus leading to a decrease in C<sub>8</sub>H<sub>13</sub>O<sub>8</sub>-RO<sub>2</sub> concentration.  
 336 Besides, it can be seen that the increasing extent in C<sub>8</sub>H<sub>13</sub>O<sub>6</sub>-RO<sub>2</sub> is also relatively small before the  
 337 NO concentration reaches 3 ppb (Figure 5c), indicating that the promotion effect of NO on C<sub>8</sub>H<sub>13</sub>O<sub>6</sub>-



338 RO<sub>2</sub> formation is not that strong at this concentration.



339

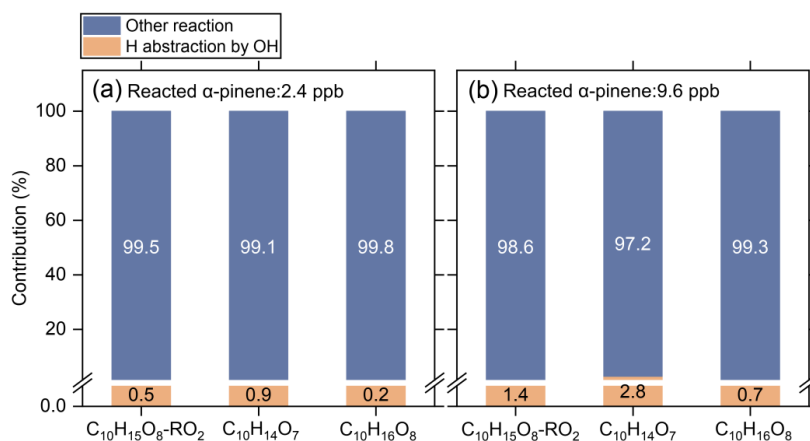
340 Figure 5 Averaged normalized concentration of typical acyl RO<sub>2</sub> as a function of initial NO or NO<sub>2</sub>  
 341 addition (Exps 1-28 and 33-56).

342 It is interesting to note that most of the measured highly oxygenated acyl RO<sub>2</sub> are formed by the  
 343 autoxidation of aldehydic RO<sub>2</sub>, and only the C<sub>8</sub>H<sub>13</sub>O<sub>9</sub>-RO<sub>2</sub> is formed by the H-shift of the RO radical  
 344 (Figure S9). The concentration of acyl RO<sub>2</sub> from the autoxidation pathway accounts for 96% of all  
 345 highly oxygenated acyl RO<sub>2</sub> concentrations. Considering that the acyl RO<sub>2</sub> with small molecular  
 346 size are generally the ring-opened RO<sub>2</sub>, the autoxidation rate constant of their precursor RO<sub>2</sub> is  
 347 expected to be relatively high (e.g., 1 s<sup>-1</sup>) (Iyer et al., 2021). Taking a RO<sub>2</sub> cross-reaction rate  
 348 constant of 1 × 10<sup>-12</sup> cm<sup>3</sup> molecule<sup>-1</sup> s<sup>-1</sup> (Zhao et al., 2018) and a model-predicted total RO<sub>2</sub>  
 349 concentration of 1.7 ppb (Exp 8), autoxidation and cross-reactions contribute to 96.0% and 4.0% of  
 350 the total RO<sub>2</sub> reaction, respectively. Considering a 10 times larger RO<sub>2</sub> cross-reaction rate constant  
 351 (i.e., 1 × 10<sup>-11</sup> cm<sup>3</sup> molecule<sup>-1</sup> s<sup>-1</sup>), the contributions of RO<sub>2</sub> autoxidation and cross-reactions would  
 352 be 70.4% and 29.6%, respectively. These calculations suggest that the autoxidation of aldehydic  
 353 RO<sub>2</sub> plays a dominant role in the formation of the highly oxygenated acyl RO<sub>2</sub>. Although the acyl  
 354 RO<sub>2</sub> with low oxygen content were not measured in this study, all acyl RO<sub>2</sub> containing oxygen atoms  
 355 less than 6 seem to be derived from the cleavage of C-C bond or H-shift of RO containing an α-  
 356 ketone or aldehyde in the currently known reaction mechanisms (Figures 4 and S10).

357 Recently, Shen et al. (2022) found that the hydrogen abstraction by OH radicals during α-pinene  
 358 oxidation plays an important role in HOM formation. In such mechanisms, the primary RO<sub>2</sub> reacts



359 with NO and forms RO radicals, which could undergo rapid ring-breaking reactions to form a series  
 360 of ring-opened  $C_{10}H_{15}O_x-RO_2$ , which contains aldehyde functionality and can easily autoxidize to  
 361  $C_{10}$  acyl  $RO_2$ . In the absence of NO, the cross-reactions of  $RO_2$  can also produce RO radicals.  
 362 However, only a few  $C_{10}$  acyl  $RO_2$  were detected in this study and they contribute less than 1% of  
 363 the total  $C_{10}$   $RO_2$  concentration. This phenomenon could be due to the fact that the primary  $RO_2$   
 364 ( $C_{10}H_{15}O_2$ ) formed by the hydrogen abstraction by OH radical are least-oxidized with only 2 oxygen  
 365 atoms, which are expected to have a relatively low cross-reaction rate constant (Orlando and Tyndall,  
 366 2012; Berndt et al., 2018). As a result, the formation of ring-opened  $C_{10}H_{15}O_x-RO_2$  via cross-  
 367 reactions of the primary  $C_{10}H_{15}O_2-RO_2$  may not be important. As shown in Figure 6, when the cross-  
 368 reaction rate constants of  $C_{10}H_{15}O_2-RO_2$  is considered to be  $1 \times 10^{-13} \text{ cm}^3 \text{ molecule}^{-1} \text{ s}^{-1}$ , the simulated  
 369 contribution of the H-abstraction pathway to the HOM formation is less than 3% under both low  
 370 (2.4 ppb) and high (9.6 ppb) reacted  $\alpha$ -pinene conditions. It should be note that the cross-reaction  
 371 rate constants of the less-oxygenated  $RO_2$  could be even lower (Orlando and Tyndall, 2012),  
 372 therefore the contribution of this pathway to HOM formation could be ignored when NO is absent.



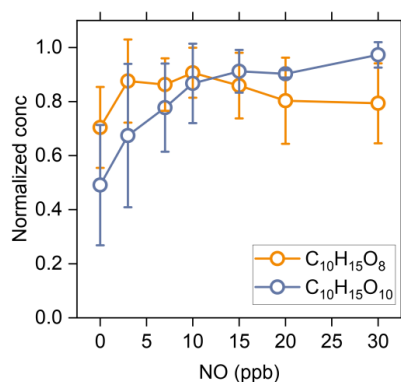
373

374 Figure 6 Contributions of the H-abstraction pathways by OH radicals (yellow) and OH addition and  
 375 ozonolysis pathways (blue) to the formation of typical HOMs under low (a) and high (b) reacted  $\alpha$ -  
 376 pinene conditions simulated by the kinetic model. The cross-reaction rate constant was set to  $1 \times 10^{-13}$   
 377  $\text{cm}^3 \text{ molecule}^{-1} \text{ s}^{-1}$  for the primary  $C_{10}H_{15}O_2-RO_2$  and  $1 \times 10^{-12} \text{ cm}^3 \text{ molecule}^{-1} \text{ s}^{-1}$  for the more  
 378 oxygenated  $RO_2$ .

379 In the presence of cyclohexane as an OH scavenger (Figure S11, Exp 32), the concentrations of  
 380  $C_{10}H_{17}O_x-RO_2$  formed via OH addition channel and the corresponding  $C_{10}H_{18}O_x$ -HOMs decrease  
 381 by more than 70%, while the  $C_{10}H_{15}O_x-RO_2$  and its related closed-shell products decrease by less  
 382 than 15%, in good agreement with the measurements in previous studies (Zhao et al., 2018). As the



383  $C_{10}H_{16}O_8$ -HOM could come from both  $C_{10}H_{15}O_x$ -RO<sub>2</sub> and  $C_{10}H_{17}O_x$ -RO<sub>2</sub>, its reduction is at a  
 384 medium level. The significantly smaller decrease in the concentrations of  $C_{10}H_{15}O_x$ -RO<sub>2</sub> and its  
 385 corresponding closed-shell products as compared to those of  $C_{10}H_{17}O_x$ -RO<sub>2</sub> and the related closed-  
 386 shell products further illustrates that the H-abstraction by OH has a minor contribution to HOM  
 387 formation in the absence of NO.



388

389 Figure 7 Averaged normalized concentration of the measured  $C_{10}H_{15}O_8$ - and  $C_{10}H_{15}O_{10}$ -RO<sub>2</sub> as a  
 390 function of the added NO concentration (Exps 33-56).

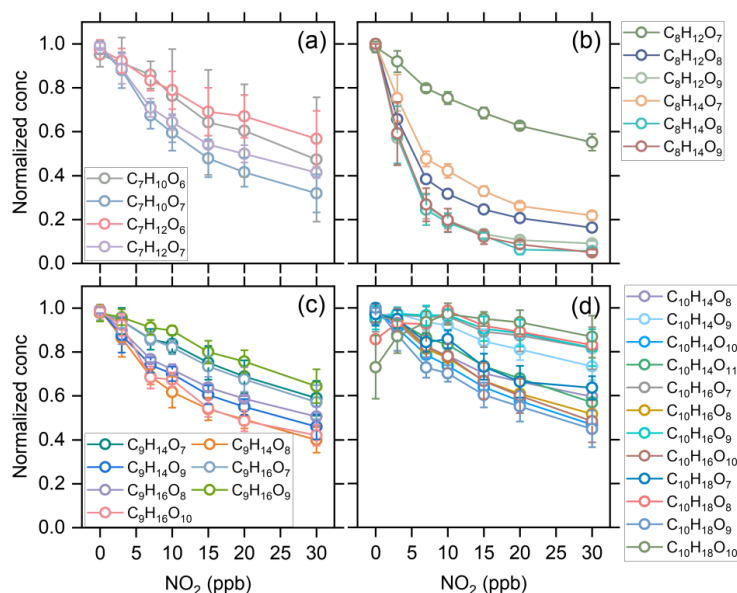
391 Figure 7 shows the changes in measured concentration of  $C_{10}H_{15}O_8$ -RO<sub>2</sub> and  $C_{10}H_{15}O_{10}$ -RO<sub>2</sub> as a  
 392 function of initial NO concentration (Exps 33-56). It should be noted that due to the existence of O<sub>3</sub>  
 393 in our experiments, these two RO<sub>2</sub> could come from both O<sub>3</sub> and OH reactions with  $\alpha$ -pinene and  
 394 NO could be rapidly oxidized to NO<sub>2</sub> by O<sub>3</sub>. The normalized concentrations of  $C_{10}H_{15}O_8$ -RO<sub>2</sub> and  
 395  $C_{10}H_{15}O_{10}$ -RO<sub>2</sub> increase firstly under low NO conditions, which is similar to the change of acyl RO<sub>2</sub>  
 396 as shown in Figure 5. This increase could be due to two reasons: (1) the promoted formation of  
 397  $C_{10}H_{15}O_8$  and  $C_{10}H_{15}O_{10}$  acyl RO<sub>2</sub> from the H-abstraction channel by NO addition and (2) the  
 398 equilibrium decomposition of ROONO<sub>2</sub> formed by the two alkyl RO<sub>2</sub> from ozonolysis of  $\alpha$ -pinene  
 399 in the CI inlet (see Section 3.1). As mentioned above, the ring-opened  $C_{10}H_{15}O_x$ -RO<sub>2</sub> formed from  
 400 the H-abstraction channel contain aldehyde functionality and can autoxidize rapidly. The FOAM  
 401 model simulations show that the  $C_{10}H_{15}O_8$  and  $C_{10}H_{15}O_{10}$  acyl RO<sub>2</sub> formed from the H-abstraction  
 402 channel contribute to 68% and 56% of the total  $C_{10}H_{15}O_8$ -RO<sub>2</sub> and  $C_{10}H_{15}O_{10}$ -RO<sub>2</sub> with the addition  
 403 of 10 ppb NO, respectively. Therefore, the initial increases of these two RO<sub>2</sub> with increasing NO  
 404 concentration are likely mainly due to the enhanced formation of  $C_{10}H_{15}O_8$  and  $C_{10}H_{15}O_{10}$  acyl RO<sub>2</sub>.  
 405 When the NO concentration increases to a high level, there are more NO and NO<sub>2</sub> in the system,  
 406 which promotes the consumption of acyl RO<sub>2</sub>. As a result,  $C_{10}H_{15}O_8$ -RO<sub>2</sub> exhibits a decreasing trend  
 407 and the increasing extend of  $C_{10}H_{15}O_{10}$ -RO<sub>2</sub> becomes much smaller.





408 **3.3 Contributions of acyl RO<sub>2</sub> to the formation of gas-phase HOMs**

409 With the addition of NO<sub>2</sub>, the distribution of gas-phase products in the α-pinene ozonolysis changes  
 410 significantly (see Figure 1), and the consumption of acyl RO<sub>2</sub> by NO<sub>2</sub> plays an important role. NO<sub>2</sub>  
 411 influences the formation of HOM monomers mainly in three ways. Firstly, NO<sub>2</sub> could react rapidly  
 412 with acyl RO<sub>2</sub> and form RC(O)OONO<sub>2</sub>, thus inhibiting the formation of HOMs with the  
 413 involvement of acyl RO<sub>2</sub>. Secondly, as mentioned above, although ROONO<sub>2</sub> is thermally unstable,  
 414 their formation/decomposition equilibrium still consumes a small amount of alkyl RO<sub>2</sub>, resulting in  
 415 a decrease in HOM formation. Thirdly, NO<sub>2</sub> can consume a part of HO<sub>2</sub> radicals (Figure S12, thus  
 416 inhibiting the RO<sub>2</sub> + HO<sub>2</sub> reaction pathway.



417  
 418 Figure 8 Averaged normalized concentration of the measured C<sub>7</sub>-C<sub>10</sub> HOMs as a function of the  
 419 added NO<sub>2</sub> concentration (Exps 1-28).

420 Figure 8 shows the normalized concentration of C<sub>7</sub>-C<sub>10</sub> HOM monomers as a function of initial NO<sub>2</sub>  
 421 concentration. The C<sub>7</sub>, C<sub>8</sub>, and some of C<sub>9</sub> HOMs decrease significantly with increasing NO<sub>2</sub>  
 422 concentration due to the relatively large contribution of acyl RO<sub>2</sub> to the total C<sub>7</sub>-C<sub>9</sub> RO<sub>2</sub>. The C<sub>7</sub>  
 423 HOMs decrease by more than 50% when the NO<sub>2</sub> concentration reaches 30 ppb, while C<sub>8</sub> HOMs  
 424 decrease by more than 70% and some of them even decrease by 90%. The C<sub>9</sub> HOMs decrease by  
 425 30%-60% and the species with relatively large decrease are mostly acyl RO<sub>2</sub>-related HOMs. For  
 426 C<sub>10</sub> HOMs, although there is also an obvious decrease in their formation with the addition of NO<sub>2</sub>,  
 427 most of them have a smaller decreasing extent compared to the C<sub>7</sub>-C<sub>9</sub> HOMs due to the low



428 contribution of acyl RO<sub>2</sub> to the C<sub>10</sub> RO<sub>2</sub>. It is worth noting that a few C<sub>10</sub> HOMs increase initially  
429 with the addition of NO<sub>2</sub> up to 10 ppb, suggesting that there might be some processes that promote  
430 the formation of their precursor RO<sub>2</sub> radicals and thus offset the inhibiting effect of NO<sub>2</sub>.

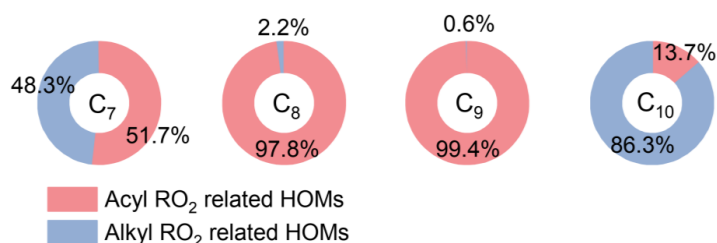
431 As mentioned above, the addition of NO<sub>2</sub> has the most significant influence on the formation of  
432 small HOM monomers. Combined with the large contribution (67-94%) of acyl RO<sub>2</sub> to the total C<sub>7</sub>  
433 and C<sub>8</sub> RO<sub>2</sub> (Figure 3), it can be considered that the reduction in the formation of C<sub>7</sub> and C<sub>8</sub> HOM  
434 monomers with NO<sub>2</sub> addition is overwhelmingly due to the consumption of acyl RO<sub>2</sub> by NO<sub>2</sub>. As a  
435 result, acyl RO<sub>2</sub> was found to have a contribution of 50-90% to C<sub>7</sub> and C<sub>8</sub> HOM monomer formation  
436 during  $\alpha$ -pinene ozonolysis. Since acyl RO<sub>2</sub> also have a considerable contribution (32%) to the total  
437 C<sub>9</sub> RO<sub>2</sub>, an upper limit (30%-60%) of its contribution to C<sub>9</sub> HOMs could be derived with the  
438 assumption that the decrease of C<sub>9</sub> HOMs with the addition of NO<sub>2</sub> is also mainly due to the  
439 consumption of C<sub>9</sub>-acyl RO<sub>2</sub> by NO<sub>2</sub>. By contrast, acyl RO<sub>2</sub> account for a very small fraction (0.5%)  
440 of the total C<sub>10</sub> RO<sub>2</sub>, and their contribution to C<sub>10</sub> HOMs cannot be quantified based solely on the  
441 experimental measurements given that the equilibrium reaction between alkyl RO<sub>2</sub> and NO<sub>2</sub> can  
442 also affect the formation of HOMs. Therefore, we used the FOAM model to simulate the contribution  
443 of acyl RO<sub>2</sub> to C<sub>10</sub> HOM formation according to the acyl RO<sub>2</sub> measured in this study and displayed  
444 the results in Figure 9. It should be noted that the HOMs from the acyl RO<sub>2</sub> and its subsequent RO<sub>2</sub>  
445 (formed from acyl RO<sub>2</sub> reactions) are all considered as acyl RO<sub>2</sub>-related HOMs in the model.

446 As mentioned above, the formation of ring-opened C<sub>10</sub>H<sub>15</sub>O<sub>4</sub>-RO<sub>2</sub> reported by Iyer et al. (2021) is  
447 included in the model, and its autoxidation produces a ring-opened acyl C<sub>10</sub>H<sub>15</sub>O<sub>8</sub>-RO<sub>2</sub>. When we  
448 considered the upper limit of the yield of ring-opened C<sub>10</sub>H<sub>15</sub>O<sub>4</sub>-RO<sub>2</sub> (89%) in the model and  
449 assumes that the other primary RO<sub>2</sub> with the cyclobutyl ring autoxidize at a very slow rate (0.01 s<sup>-1</sup>)  
450 <sup>1</sup>), the simulated acyl C<sub>10</sub>H<sub>15</sub>O<sub>8</sub>-RO<sub>2</sub> would contribute to ~80% of the total C<sub>10</sub> RO<sub>2</sub>. However, we  
451 could not see a large decrease in the measured concentration of C<sub>10</sub>H<sub>15</sub>O<sub>8</sub>-RO<sub>2</sub> and its related HOM  
452 monomers with the addition of NO<sub>2</sub>. Similarly, a recent study by Zhao et al. (2022) found that the  
453 C<sub>10</sub>H<sub>15</sub>O<sub>8</sub>-related monomers and dimers in  $\alpha$ -pinene SOA also did not show significant decreases  
454 with NO<sub>2</sub> addition. There might be two reasons for the discrepancy between the simulations and  
455 measurements. Firstly, the yield of the ring-opened C<sub>10</sub>H<sub>15</sub>O<sub>4</sub>-RO<sub>2</sub> might be significantly smaller  
456 than 89% (Zhao et al., 2021; Meder et al., 2023). Secondly, the autoxidation rate of other primary  
457 C<sub>10</sub>H<sub>15</sub>O<sub>4</sub>-RO<sub>2</sub> with the cyclobutyl ring could be significantly larger than 0.01 s<sup>-1</sup>. Therefore, we  
458 updated the branching ratios and autoxidation rates of the primary RO<sub>2</sub> during the  $\alpha$ -pinene  
459 ozonolysis in the model according to the recent studies (Kurten et al., 2015; Clafin et al., 2018;  
460 Zhao et al., 2021; Berndt, 2022) (Table S3), and a lower limit (30%) of the ring-opened C<sub>10</sub>H<sub>15</sub>O<sub>4</sub>-



461 RO<sub>2</sub> yield reported by Iyer et al. (2021) was used here. The simulated acyl RO<sub>2</sub>-related HOMs  
 462 contribute to 14% of the total C<sub>10</sub> HOMs, which is slightly smaller than the measured decrease in  
 463 C<sub>10</sub> HOMs with the addition of NO<sub>2</sub>. This discrepancy could be due to two reasons. Firstly, the  
 464 decrease in HOMs can partly result from the consumption of alkyl RO<sub>2</sub> and HO<sub>2</sub> radicals by the  
 465 addition of NO<sub>2</sub>. Secondly, as mentioned above, there might be other C<sub>10</sub> acyl RO<sub>2</sub> that were not  
 466 observed in this study due to the decomposition of the ROONO<sub>2</sub> from the alkyl RO<sub>2</sub> with the same  
 467 formulas.

468 The contributions of acyl RO<sub>2</sub> to the formation of C<sub>7</sub>-C<sub>9</sub> HOMs were also simulated (Figure 9). For  
 469 C<sub>7</sub> and C<sub>8</sub> HOMs, the model predicts a contribution of 52%-98% from acyl RO<sub>2</sub>, which is consistent  
 470 with the measurements (50%-90%). However, the simulated contribution of acyl RO<sub>2</sub> to C<sub>9</sub> HOMs  
 471 is over 99%, which is not consistent with the measurements (Figure 8c). Recent studies indicated  
 472 that the CI radicals from α-pinene ozonolysis could not form the alkyl C<sub>9</sub>H<sub>15</sub>O<sub>3</sub>-RO<sub>2</sub> (C96O2 in  
 473 default MCM v3.3.1) (Kurten et al., 2015; Zhao et al., 2021; Berndt, 2022). As a result, this primary  
 474 C<sub>9</sub> alkyl RO<sub>2</sub> was not considered in the model, and most of C<sub>9</sub> RO<sub>2</sub> considered are acyl RO<sub>2</sub> or from  
 475 acyl RO<sub>2</sub> reactions. In view of the significantly lower measured (less than 30-60%) than simulated  
 476 (over 99%) contribution of acyl RO<sub>2</sub> to C<sub>9</sub> HOMs, we speculate that a small part of CI radicals  
 477 might be able to form the C<sub>9</sub>H<sub>15</sub>O<sub>3</sub>-RO<sub>2</sub>, which could further react to form highly oxygenated alkyl  
 478 C<sub>9</sub> RO<sub>2</sub>.



479

480 Figure 9 Simulated average contribution of acyl and alkyl RO<sub>2</sub> to C<sub>7</sub>-C<sub>10</sub> HOM formation from  
 481 ozonolysis of α-pinene under typical experimental conditions (Exps 1, 8, 15, and 22).

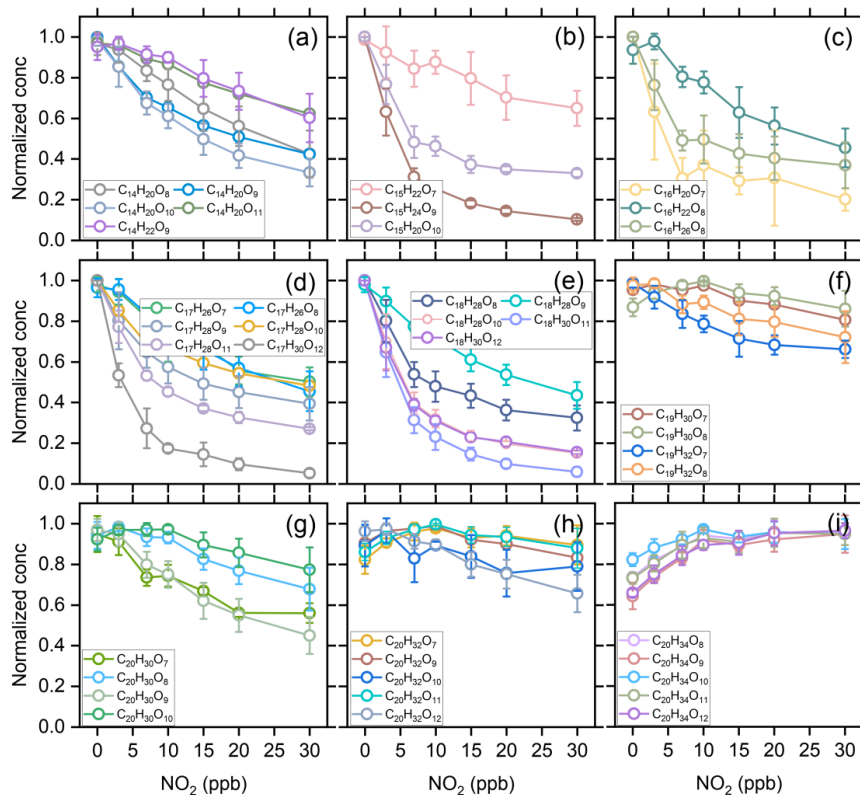
482 A sensitive analysis of the alkyl C<sub>9</sub>H<sub>15</sub>O<sub>3</sub>-RO<sub>2</sub> yield was conducted to see its influence on the  
 483 contribution of acyl RO<sub>2</sub> to the total C<sub>9</sub> HOMs. The model simulations show that when the yield of  
 484 this C<sub>9</sub> RO<sub>2</sub> from one of the CIs ranges between 0.5% to 2%, the contribution of acyl RO<sub>2</sub> to the  
 485 total C<sub>9</sub> HOMs ranges from 27.5% to 59.8% (Figure S13), which is almost consistent with the  
 486 measurements. This result indicates that a small part of CIs could generate the C<sub>9</sub> alkyl RO<sub>2</sub>.

487 The cross-reaction rate constant of acyl RO<sub>2</sub> is generally larger than that of alkyl RO<sub>2</sub> (Atkinson et



488 al., 2007; Orlando and Tyndall, 2012), and the fast cross-reaction may lead to an important  
489 contribution to the HOM dimer production. The responses of dimer formation to increasing  
490 concentration of initial NO<sub>2</sub> during  $\alpha$ -pinene ozonolysis are given in Figure 10. The C<sub>14</sub>-C<sub>18</sub> dimers  
491 decrease by up to 50%-95% with the increase of NO<sub>2</sub> concentration up to 30 ppb (Figures 10a-e).  
492 The rapid cross-reaction rate of acyl RO<sub>2</sub>, as well as their dominant contribution to the small RO<sub>2</sub>  
493 species makes acyl RO<sub>2</sub> an important contributor to the formation of these dimers. The consumption  
494 of acyl RO<sub>2</sub> by NO<sub>2</sub> greatly inhibits the bimolecular reactions involving acyl RO<sub>2</sub>, resulting in a  
495 rapid decrease in the concentration of the corresponding dimers. Considering the predominance of  
496 acyl RO<sub>2</sub> in small RO<sub>2</sub> and their high reaction rate with NO<sub>2</sub> compared to the alkyl RO<sub>2</sub>, it can be  
497 concluded that the cross-reactions involving acyl RO<sub>2</sub> contribute to roughly 50%-95% of the C<sub>14</sub>-  
498 C<sub>18</sub> dimer formation.

499 For C<sub>19</sub> dimers, due to the relatively smaller contribution of acyl RO<sub>2</sub> to C<sub>9</sub> and C<sub>10</sub> RO<sub>2</sub>, their  
500 concentration decreases only by 10%-40%, and this reduction have contributions from both acyl  
501 and alkyl RO<sub>2</sub>. For C<sub>20</sub> dimers, their concentration changes with the addition of NO<sub>2</sub> can be  
502 discussed according to the number of hydrogen atoms in the molecules. Firstly, the concentration  
503 of C<sub>20</sub>H<sub>30</sub>O<sub>7</sub> and C<sub>20</sub>H<sub>30</sub>O<sub>9</sub> decreases by 40-60% with the addition of 30 ppb NO<sub>2</sub>, indicating a  
504 significant contribution of acyl RO<sub>2</sub> such as C<sub>10</sub>H<sub>15</sub>O<sub>5</sub>-RO<sub>2</sub> (acyl RO<sub>2</sub> in default MCM v3.3.1) and  
505 C<sub>10</sub>H<sub>15</sub>O<sub>7</sub>-RO<sub>2</sub> in their formation, while other C<sub>20</sub>H<sub>30</sub>O<sub>x</sub> dimers decrease by ~30%. The C<sub>20</sub>H<sub>32</sub>O<sub>x</sub>  
506 dimer series also exhibits a small reduction (less than 20%) with the addition of NO<sub>2</sub>. However, the  
507 C<sub>20</sub>H<sub>34</sub>O<sub>x</sub> series shows an unexpected increase with the addition of NO<sub>2</sub> up to 10 ppb and almost  
508 remains unchanged with the further increase of NO<sub>2</sub> concentration. Given that the cross-reaction  
509 rate constant of acyl RO<sub>2</sub> can be orders of magnitude higher than that of counterpart alkyl RO<sub>2</sub>  
510 (Atkinson et al., 2007; Orlando and Tyndall, 2012), the rapid consumption of acyl RO<sub>2</sub> by NO<sub>2</sub>  
511 would preserve the alkyl RO<sub>2</sub> that tend to react with acyl RO<sub>2</sub> at a fast rate in the absence of NO<sub>2</sub>,  
512 which to some extent would elevate the concentration of alkyl RO<sub>2</sub> in the system and thus promote  
513 the less competitive alkyl RO<sub>2</sub> + alkyl RO<sub>2</sub> reactions to form C<sub>20</sub>H<sub>34</sub>O<sub>x</sub> dimers. The slight increase  
514 of some C<sub>10</sub>H<sub>18</sub>O<sub>x</sub>-HOMs with the addition of NO<sub>2</sub> up to 10 ppb could also be due to this reason.



515

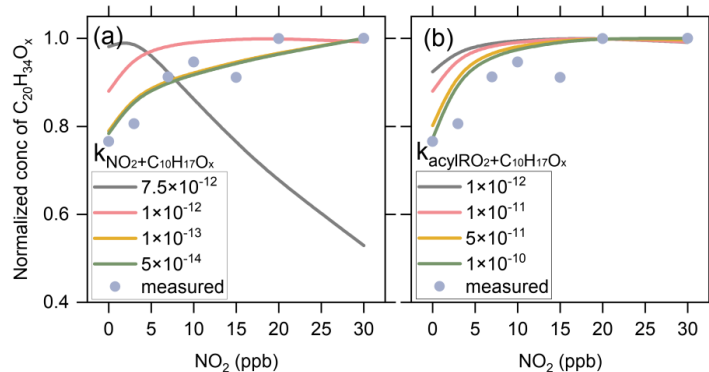
516 Figure 10 Averaged normalized concentration of the measured C<sub>14</sub>-C<sub>20</sub> dimers as a function of the  
 517 added NO<sub>2</sub> concentration (Exps 1-28).

518 According to the noticeable increasing trend in C<sub>20</sub>H<sub>34</sub>O<sub>x</sub> as compared to other C<sub>20</sub> dimers, we  
 519 speculate that acyl RO<sub>2</sub> react faster with C<sub>10</sub>H<sub>17</sub>O<sub>x</sub> alkyl RO<sub>2</sub> than with C<sub>10</sub>H<sub>15</sub>O<sub>x</sub> alkyl RO<sub>2</sub>.  
 520 Therefore, when the acyl RO<sub>2</sub> is depleted, the preservation of C<sub>10</sub>H<sub>17</sub>O<sub>x</sub>-RO<sub>2</sub> is more significant and  
 521 the promotion of their cross-reactions to form C<sub>20</sub>H<sub>34</sub>O<sub>x</sub> is more evident. It is also possible that the  
 522 reaction of NO<sub>2</sub> with C<sub>10</sub>H<sub>17</sub>O<sub>x</sub> alkyl RO<sub>2</sub> is less efficient compared to the reaction with C<sub>10</sub>H<sub>15</sub>O<sub>x</sub>  
 523 alkyl RO<sub>2</sub>, so more C<sub>10</sub>H<sub>17</sub>O<sub>x</sub> than C<sub>10</sub>H<sub>15</sub>O<sub>x</sub> are available for dimer formation in the presence of  
 524 NO<sub>2</sub>.

525 To further prove the above two speculations, we performed sensitivity analyses for the reaction rates  
 526 of C<sub>10</sub>H<sub>17</sub>O<sub>x</sub>-RO<sub>2</sub> using the F0AM model. Figures 11a show the changes in C<sub>20</sub>H<sub>34</sub>O<sub>x</sub> dimers with  
 527 NO<sub>2</sub> addition at different C<sub>10</sub>H<sub>17</sub>O<sub>x</sub>-RO<sub>2</sub> + NO<sub>2</sub> reaction rates under the conditions of Exps 8-14. As  
 528 the reaction rate varies from 5 × 10<sup>-14</sup> to 1 × 10<sup>-12</sup> cm<sup>3</sup> molecule<sup>-1</sup> s<sup>-1</sup>, the increasing trend of C<sub>20</sub>H<sub>34</sub>O<sub>x</sub>  
 529 dimers versus the added NO<sub>2</sub> concentration is significantly weakened and the simulations are more



530 deviated from the measurements. When the reaction rate increases to  $7.5 \times 10^{-12} \text{ cm}^3 \text{ molecule}^{-1} \text{ s}^{-1}$ ,  
 531 the  $\text{C}_{20}\text{H}_{34}\text{O}_x$  dimers decrease significantly with increasing  $\text{NO}_2$ , which is in striking contrast to the  
 532 measurements. Figure 11b presents the sensitivity analysis results for the cross-reaction rate  
 533 constants of acyl  $\text{RO}_2 + \text{C}_{10}\text{H}_{17}\text{O}_x\text{-RO}_2$ . As this rate constant varies from  $1 \times 10^{-12}$  to  $1 \times 10^{-10} \text{ cm}^3$   
 534  $\text{molecule}^{-1} \text{ s}^{-1}$ , the increasing trend of  $\text{C}_{20}\text{H}_{34}\text{O}_x$  versus the  $\text{NO}_2$  concentration is more pronounced  
 535 and more consistent with the measurements. These sensitivity analyses support our speculation that  
 536 the  $\text{C}_{10}\text{H}_{17}\text{O}_x$  alkyl  $\text{RO}_2$  may be different from other alkyl  $\text{RO}_2$  radicals in terms of the reaction  
 537 efficiency with  $\text{NO}_2$  and acyl  $\text{RO}_2$  species, which leads to different responses of  $\text{C}_{20}\text{H}_{34}\text{O}_x$  dimers  
 538 to  $\text{NO}_2$  addition compared to other  $\text{C}_{20}$  dimers. These results also suggest that the presence of acyl  
 539  $\text{RO}_2$  could affect the fate and contribution of alkyl  $\text{RO}_2$  to HOM formation in atmospheric oxidation  
 540 systems given the different reactivity of acyl  $\text{RO}_2$  from alkyl  $\text{RO}_2$ .



541  
 542 Figure 11 Sensitivity analyses of the reaction rates of  $\text{NO}_2$  with  $\text{C}_{10}\text{H}_{17}\text{O}_x\text{-RO}_2$  (a), and the cross-  
 543 reaction rate of acyl  $\text{RO}_2$  with  $\text{C}_{10}\text{H}_{17}\text{O}_x\text{-RO}_2$  (b), considering a rate of  $1 \times 10^{-12} \text{ cm}^3 \text{ molecule}^{-1} \text{ s}^{-1}$   
 544 for  $\text{C}_{10}\text{H}_{17}\text{O}_x\text{-RO}_2 + \text{NO}_2$ .

#### 545 4. Conclusions

546 In this study, the molecular identities, formation mechanisms, and contributions of acyl  $\text{RO}_2$  to the  
 547 formation of HOMs during ozonolysis of  $\alpha$ -pinene are investigated using a combination of flow  
 548 reactor experiments and detailed kinetic model simulations. Based on the marked decrease in  $\text{RO}_2$   
 549 concentration as a function of initial  $\text{NO}_2$  concentration, a total of 10 acyl  $\text{RO}_2$  are identified during  
 550  $\alpha$ -pinene ozonolysis. The acyl  $\text{RO}_2$  contributes to 67%, 94% and 32% of  $\text{C}_7$ ,  $\text{C}_8$  and  $\text{C}_9$  highly  
 551 oxygenated  $\text{RO}_2$  but only 0.5% of  $\text{C}_{10}$  highly oxygenated  $\text{RO}_2$ , respectively. Three main pathways  
 552 are identified for the formation of monoterpene-derived acyl  $\text{RO}_2$ : (i) the autoxidation of  $\text{RO}_2$   
 553 containing aldehyde groups, (ii) the cleavage of C-C bond of  $\text{RO}$  containing an  $\alpha$ -ketone group, and  
 554 (iii) the intramolecular H-shift of  $\text{RO}$  containing an aldehyde group. The autoxidation of aldehydic



555 RO<sub>2</sub> formed involving multiple RO decomposition or ring-opening steps plays a dominant role in  
556 the formation of the highly oxygenated acyl RO<sub>2</sub> radicals (oxygen atom number  $\geq 6$ ), while the  
557 less-oxygenated acyl RO<sub>2</sub> (oxygen atom number  $< 6$ ) are mainly derived from the other two  
558 pathways.

559 The acyl RO<sub>2</sub>-involved reactions explain 50-90% of C<sub>7</sub> and C<sub>8</sub> HOM monomers and 14% of C<sub>10</sub>  
560 HOMs, respectively. For C<sub>9</sub> HOMs, this contribution can be up to 30%-60%. For the HOM dimers,  
561 acyl RO<sub>2</sub>-involved reactions contribute 50%-95% to the formation of C<sub>14</sub>-C<sub>18</sub> dimers. Owing to the  
562 higher cross-reaction rate constant of acyl RO<sub>2</sub> compared to alkyl RO<sub>2</sub>, the acyl RO<sub>2</sub> + alkyl RO<sub>2</sub>  
563 reaction would outcompete the alkyl RO<sub>2</sub> + alkyl RO<sub>2</sub> reaction. Therefore, the rapid consumption  
564 of acyl RO<sub>2</sub> by NO<sub>2</sub> in the experiments (as well as in polluted atmospheres) would make the alkyl  
565 RO<sub>2</sub> that are supposed to react with acyl RO<sub>2</sub> retained, which to some extent elevates the  
566 concentration of alkyl RO<sub>2</sub> in the system and thus promotes the reaction of alkyl RO<sub>2</sub> + alkyl RO<sub>2</sub>  
567 to form dimers such as C<sub>20</sub>H<sub>34</sub>O<sub>x</sub>. The contribution of H-abstraction of  $\alpha$ -pinene by OH radical to  
568 the formation of acyl RO<sub>2</sub> and HOMs is found to be negligible in the absence of NO. This is because  
569 the primary C<sub>10</sub>H<sub>15</sub>O<sub>2</sub>-RO<sub>2</sub> radicals formed in such pathways are least-oxidized and thus have  
570 relatively low cross-reaction efficiency to produce RO radicals, which are the key intermediates for  
571 the formation of acyl RO<sub>2</sub> and HOMs in that channel. However, in the presence of NO, the formation  
572 of highly oxygenated acyl RO<sub>2</sub> via the H-abstraction pathway is demonstrated, consistent with  
573 previous studies (Shen et al., 2022).

574 In this study, acyl RO<sub>2</sub> species are identified according to a dramatic decrease in their concentration  
575 with the addition of NO<sub>2</sub>. It should be noted that the presence of NO<sub>2</sub> could also inhibit the formation  
576 of alkyl RO<sub>2</sub> species involving acyl RO<sub>2</sub> reactions. If there are any contributions of alkyl RO<sub>2</sub> to  
577 acyl RO<sub>2</sub> identified in this study, the influence of such alkyl RO<sub>2</sub> species on HOM formation would  
578 reflect an indirect effect of acyl RO<sub>2</sub>. However, given that the formation of most of the acyl RO<sub>2</sub>  
579 identified in this study can be reasonably explained by the proposed mechanisms and verified by  
580 their responses to the addition of NO, the acyl RO<sub>2</sub> identified here are expected to have no significant  
581 contributions from alkyl RO<sub>2</sub>. Currently, the reaction kinetics of monoterpene-derived acyl RO<sub>2</sub> are  
582 still poorly understood. Considering the important contribution of acyl RO<sub>2</sub> to HOM formation,  
583 further kinetic studies are needed to get more specific rate constants for their autoxidation and cross-  
584 reactions, thereby deepening our understanding of the role of acyl RO<sub>2</sub> in HOM and SOA formation  
585 under atmospheric conditions.

586

587 *Data availability.* The data presented in this work are available upon request from the corresponding  
588 author.





589

590 *Author contributions.* YZ and HZ designed the study, HZ, DH and JZ performed the experiments.  
591 YZ and HZ analyzed the data, conducted model simulations, and wrote the paper. All other authors  
592 contributed to discussion and writing.

593

594 *Competing interests.* The authors declare no conflict of interest.

595

596 *Acknowledgments.* Yue Zhao acknowledges the Program for Professor of Special  
597 Appointment (Eastern Scholar) at Shanghai Institutions of Higher Learning.

598

599 *Financial support.* This work was supported by the National Natural Science Foundation  
600 of China (grants 22022607, 21806104, and 42005090) and the Program for Professor of  
601 Special Appointment (Eastern Scholar) at Shanghai Institutions of Higher Learning.

602

## 603 **References**

604 Atkinson, R., Hasegawa, D., and Aschmann, S. M.: Rate constants for the gas-phase reactions of O<sub>3</sub> with  
605 a series of monoterpenes and related compounds at 296 ± 2 K, *Int. J. Chem. Kinet.*, 1221,  
606 <https://doi.org/10.1002/kin.550220807>, 1990.

607 Atkinson, R., Baulch, D., Cox, R., Crowley, J., Hampson, R., Hynes, R., Jenkin, M., Rossi, M., and Troe,  
608 J.: Evaluated kinetic and photochemical data for atmospheric chemistry: Volume III–gas phase  
609 reactions of inorganic halogens, *Atmos. Chem. Phys.*, 7, 981-1191, [https://doi.org/10.5194/acp-7-](https://doi.org/10.5194/acp-7-981-2007)  
610 981-2007, 2007.

611 Bell, D. M., Wu, C., Bertrand, A., Graham, E., Schoonbaert, J., Giannoukos, S., Baltensperger, U., Prevot,  
612 A., Riipinen, I., and Haddad, I. E.: Particle-phase processing of  $\alpha$ -pinene NO<sub>3</sub> secondary organic  
613 aerosol in the dark, *Atmos. Chem. Phys.*, 13167–13182, <https://doi.org/10.5194/acp-22-13167-2022>,  
614 2021.

615 Berndt, T.: Peroxy radical processes and product formation in the OH radical-initiated oxidation of alpha-  
616 pinene for near-atmospheric conditions, *J. Phys. Chem. A*, 125, 9151-9160,  
617 <https://doi.org/10.1021/acs.jpca.1c05576>, 2021.

618 Berndt, T.: Peroxy radical and product formation in the gas-phase ozonolysis of alpha-pinene under near-  
619 atmospheric conditions: occurrence of an additional series of peroxy radicals O<sub>2</sub>C<sub>10</sub>H<sub>15</sub>O(O<sub>2</sub>)<sub>y</sub>O<sub>2</sub> with y = 1-3, *J. Phys. Chem. A*, 126, 6526-6537,  
620 <https://doi.org/10.1021/acs.jpca.2c05094>, 2022.

622 Berndt, T., Mentler, B., Scholz, W., Fischer, L., Herrmann, H., Kulmala, M., and Hansel, A.: Accretion  
623 product formation from ozonolysis and OH radical reaction of alpha-pinene: mechanistic insight and  
624 the influence of isoprene and ethylene, *Environ. Sci. Technol.*, 52, 11069-11077,  
625 <https://doi.org/10.1021/acs.est.8b02210>, 2018.

626 Berndt, T., Richters, S., Jokinen, T., Hyttinen, N., Kurtén, T., Otkjær, R. V., Kjaergaard, H. G., Stratmann,  
627 F., Herrmann, H., and Sipilä, M.: Hydroxyl radical-induced formation of highly oxidized organic  
628 compounds, *Nat. Commun.*, 7, 1-8, <https://doi.org/10.1038/ncomms13677>, 2016.

629 Bianchi, F., Kurtén, T., Riva, M., Mohr, C., Rissanen, M. P., Roldin, P., Berndt, T., Crouse, J. D.,  
630 Wennberg, P. O., and Mentel, T. F.: Highly oxygenated organic molecules (HOM) from gas-phase





- 631 autoxidation involving peroxy radicals: A key contributor to atmospheric aerosol, *Chem. Rev.*, 119,  
632 3472-3509, 2019.
- 633 Calvert, J. G., Derwent, R. G., Orlando, J. J., Wallington, T. J., and Tyndall, G. S.: Mechanisms of  
634 atmospheric oxidation of the alkanes, 2008.
- 635 Claflin, M. S., Krechmer, J. E., Hu, W., Jimenez, J. L., and Ziemann, P. J.: Functional group composition  
636 of secondary organic aerosol formed from ozonolysis of  $\alpha$ -pinene under high VOC and autoxidation  
637 conditions, *ACS Earth Space Chem.*, 2, 1196-1210,  
638 <https://doi.org/10.1021/acsearthspacechem.8b00117>, 2018.
- 639 Ehn, M., Thornton, J. A., Kleist, E., Sipilä, M., Junninen, H., Pullinen, I., Springer, M., Rubach, F.,  
640 Tillmann, R., and Lee, B.: A large source of low-volatility secondary organic aerosol, *Nature*, 506,  
641 476-479, <https://doi.org/10.1038/nature13032>, 2014.
- 642 Fry, J., Kiendler-Scharr, A., Rollins, A., Wooldridge, P., Brown, S., Fuchs, H., Dubé, W., Mensah, A.,  
643 Dal Maso, M., and Tillmann, R.: Organic nitrate and secondary organic aerosol yield from NO<sub>3</sub>  
644 oxidation of  $\beta$ -pinene evaluated using a gas-phase kinetics/aerosol partitioning model, *Atmos. Chem.*  
645 *Phys.*, 9, 1431-1449, <https://doi.org/10.5194/acp-9-1431-2009>, 2009.
- 646 Fry, J. L., Draper, D. C., Barsanti, K. C., Smith, J. N., Ortega, J., Winkler, P. M., Lawler, M. J., Brown,  
647 S. S., Edwards, P. M., and Cohen, R. C.: Secondary organic aerosol formation and organic nitrate  
648 yield from NO<sub>3</sub> oxidation of biogenic hydrocarbons, *Environ. Sci. Technol.*, 48, 11944-11953,  
649 <https://doi.org/10.1021/es502204x>, 2014.
- 650 Guenther, A., Jiang, X., Heald, C. L., Sakulyanontvittaya, T., Duhl, T. a., Emmons, L., and Wang, X.:  
651 The model of emissions of gases and aerosols from nature version 2.1 (MEGAN2. 1): an extended  
652 and updated framework for modeling biogenic emissions, *Geosci. Model Dev.*, 5, 1471-1492,  
653 <https://doi.org/10.5194/gmd-5-1471-2012>, 2012.
- 654 Iyer, S., Rissanen, M. P., Valiev, R., Barua, S., Krechmer, J. E., Thornton, J., Ehn, M., and Kurten, T.:  
655 Molecular mechanism for rapid autoxidation in alpha-pinene ozonolysis, *Nat. Commun.*, 12, 878,  
656 <https://doi.org/10.1038/s41467-021-21172-w>, 2021.
- 657 Jenkin, M., Young, J., and Rickard, A.: The MCM v3.3.1 degradation scheme for isoprene, *Atmos. Chem.*  
658 *Phys.*, 15, 11433-11459, <https://doi.org/10.5194/acp-15-11433-2015>, 2015.
- 659 Jokinen, T., Sipilä, M., Junninen, H., Ehn, M., Lönn, G., Hakala, J., Petäjä, T., Mauldin, R. L., Kulmala,  
660 M., and Worsnop, D. R.: Atmospheric sulphuric acid and neutral cluster measurements using CI-  
661 APi-TOF, *Atmos. Chem. Phys.*, 12, 4117-4125, <https://doi.org/10.5194/acp-12-4117-2012>, 2012.
- 662 Jokinen, T., Sipilä, M., Richters, S., Kerminen, V. M., Paasonen, P., Stratmann, F., Worsnop, D., Kulmala,  
663 M., Ehn, M., and Herrmann, H.: Rapid autoxidation forms highly oxidized RO<sub>2</sub> radicals in the  
664 atmosphere, *Angew. Chem. Int. Ed.*, 53, 14596-14600, <https://doi.org/10.1002/anie.201408566>,  
665 2014.
- 666 Junninen, H., Ehn, M., Petäjä, T., Luosujärvi, L., Kotiaho, T., Kostianen, R., Rohner, U., Gonin, M.,  
667 Fuhrer, K., and Kulmala, M.: A high-resolution mass spectrometer to measure atmospheric ion  
668 composition, *Atmos. Meas. Tech.*, 3, 599-636, <https://doi.org/10.5194/amt-3-1039-2010>, 2010.
- 669 Kirchner, F., Thuener, L., Barnes, I., Becker, K., Donner, B., and Zabel, F.: Thermal lifetimes of  
670 peroxy nitrates occurring in the atmospheric degradation of oxygenated fuel additives, *Environ. Sci.*  
671 *Technol.*, 31, 1801-1804, <https://doi.org/10.1021/es9609415>, 1997.
- 672 Knopf, D. A., Pöschl, U., and Shiraiwa, M.: Radial diffusion and penetration of gas molecules and aerosol  
673 particles through laminar flow reactors, denuders, and sampling tubes, *Anal. Chem.*, 87, 3746-3754,  
674 <https://doi.org/10.1021/ac5042395>, 2015.



- 675 Kristensen, K., Watne, Å. K., Hammes, J., Lutz, A., Petäjä, T., Hallquist, M., Bilde, M., and Glasius, M.:  
676 High-molecular weight dimer esters are major products in aerosols from  $\alpha$ -pinene ozonolysis and  
677 the boreal forest, *Environmental Science & Technology Letters*, 3, 280-285, 2016.
- 678 Kurten, T., Rissanen, M. P., Mackeprang, K., Thornton, J. A., Hyttinen, N., Jorgensen, S., Ehn, M., and  
679 Kjaergaard, H. G.: Computational study of hydrogen shifts and ring-opening mechanisms in alpha-  
680 pinene ozonolysis products, *J. Phys. Chem. A*, 119, 11366-11375,  
681 <https://doi.org/10.1021/acs.jpca.5b08948>, 2015.
- 682 Li, X., Chee, S., Hao, J., Abbatt, J. P. D., Jiang, J., and Smith, J. N.: Relative humidity effect on the  
683 formation of highly oxidized molecules and new particles during monoterpene oxidation, *Atmos.*  
684 *Chem. Phys.*, 19, 1555-1570, <https://doi.org/10.5194/acp-19-1555-2019>, 2019.
- 685 Lin, C., Huang, R.-J., Duan, J., Zhong, H., and Xu, W.: Primary and secondary organic nitrate in  
686 northwest China: a case study, *Environ. Sci. Technol. Lett.*, 8, 947-953,  
687 <https://doi.org/10.1021/acs.estlett.1c00692>, 2021.
- 688 Meder, M., Peräkylä, O., Varelas, J. G., Luo, J., Cai, R., Zhang, Y., Kurtén, T., Riva, M., Rissanen, M.,  
689 Geiger, F. M., Thomson, R. J., and Ehn, M.: Selective deuteration as a tool for resolving autoxidation  
690 mechanisms in  $\alpha$ -pinene ozonolysis, *Atmos. Chem. Phys.*, 23, 4373-4390,  
691 <https://doi.org/10.5194/egusphere-2022-1131>, 2023.
- 692 Mentel, T., Springer, M., Ehn, M., Kleist, E., Pullinen, I., Kurtén, T., Rissanen, M., Wahner, A., and Wildt,  
693 J.: Formation of highly oxidized multifunctional compounds: autoxidation of peroxy radicals formed  
694 in the ozonolysis of alkenes—deduced from structure–product relationships, *Atmos. Chem. Phys.*, 15,  
695 6745-6765, <https://doi.org/10.5194/acp-15-6745-2015>, 2015.
- 696 Molteni, U., Simon, M., Heinritzi, M., Hoyle, C. R., Bernhammer, A.-K., Bianchi, F., Breitenlechner, M.,  
697 Brilke, S., Dias, A., Duplissy, J., Frege, C., Gordon, H., Heyn, C., Jokinen, T., Kürten, A., Lehtipalo,  
698 K., Makhmudov, V., Petäjä, T., Pieber, S. M., Praplan, A. P., Schobesberger, S., Steiner, G., Stozhkov,  
699 Y., Tomé, A., Tröstl, J., Wagner, A. C., Wagner, R., Williamson, C., Yan, C., Baltensperger, U.,  
700 Curtius, J., Donahue, N. M., Hansel, A., Kirkby, J., Kulmala, M., Worsnop, D. R., and Dommen, J.:  
701 Formation of highly oxygenated organic molecules from  $\alpha$ -pinene ozonolysis: chemical  
702 characteristics, mechanism, and kinetic model development, *ACS Earth Space Chem.*, 3, 873-883,  
703 <https://doi.org/10.1021/acsearthspacechem.9b00035>, 2019.
- 704 Noziere, B., Kalberer, M., Claeys, M., Allan, J., D'Anna, B., Decesari, S., Finessi, E., Glasius, M., Grgic,  
705 I., and Hamilton, J. F.: The molecular identification of organic compounds in the atmosphere: state  
706 of the art and challenges, *Chem. Rev.*, 115, 3919-3983, 2015.
- 707 Orlando, J. J. and Tyndall, G. S.: Laboratory studies of organic peroxy radical chemistry: an overview  
708 with emphasis on recent issues of atmospheric significance, *Chem. Soc. Rev.*, 41, 6294-6317,  
709 <https://doi.org/10.1039/C2CS35166H>, 2012.
- 710 Otkjær, R. V., Jakobsen, H. H., Tram, C. M., and Kjaergaard, H. G.: Calculated hydrogen shift rate  
711 constants in substituted alkyl peroxy radicals, *J. Phys. Chem. A*, 122, 8665-8673,  
712 <https://doi.org/10.1021/acs.jpca.8b06223>, 2018.
- 713 Pye, H., Chan, A., Barkley, M., and Seinfeld, J.: Global modeling of organic aerosol: the importance of  
714 reactive nitrogen ( $\text{NO}_x$  and  $\text{NO}_3$ ), *Atmos. Chem. Phys.*, 10, 11261-11276,  
715 <https://doi.org/10.5194/acp-10-11261-2010>, 2010.
- 716 Roger, Atkinson, Sara, M., Aschmann, James, N., Pitts, and Jr.: Rate constants for the gas-phase reactions  
717 of the OH radical with a series of monoterpenes at  $294 \pm 1$  K, *Int. J. Chem. Kinet.*, 2004.
- 718 Shen, H., Vereecken, L., Kang, S., Pullinen, I., Fuchs, H., Zhao, D., and Mentel, T. F.: Unexpected



- 719 significance of a minor reaction pathway in daytime formation of biogenic highly oxygenated  
720 organic compounds, *Sci. Adv.*, 8, eabp8702, <https://doi.org/10.1126/sciadv.abp8702>, 2022.
- 721 Sindelarova, K., Granier, C., Bouarar, I., Guenther, A., Tilmes, S., Stavrou, T., Müller, J.-F., Kuhn, U.,  
722 Stefani, P., and Knorr, W.: Global data set of biogenic VOC emissions calculated by the MEGAN  
723 model over the last 30 years, *Atmos. Chem. Phys.*, 14, 9317-9341, [https://doi.org/10.5194/acp-14-](https://doi.org/10.5194/acp-14-9317-2014)  
724 9317-2014, 2014.
- 725 Tyndall, G., Cox, R., Granier, C., Lesclaux, R., Moortgat, G., Pilling, M., Ravishankara, A., and  
726 Wallington, T.: Atmospheric chemistry of small organic peroxy radicals, *Journal of Geophysical*  
727 *Research: Atmospheres*, 106, 12157-12182, 2001.
- 728 Villenave, E. and Lesclaux, R.: Kinetics of the cross reactions of  $\text{CH}_3\text{O}_2$  and  $\text{C}_2\text{H}_5\text{O}_2$  radicals with  
729 selected peroxy radicals, *J. Phys. Chem. C*, 100, 14372-14382, <https://doi.org/10.1021/jp960765m>,  
730 1996.
- 731 Wang, Y., Zhao, Y., Li, Z., Li, C., Yan, N., and Xiao, H.: Importance of hydroxyl radical chemistry in  
732 isoprene suppression of particle formation from  $\alpha$ -pinene ozonolysis, *ACS Earth Space Chem.*, 5,  
733 487-499, <https://doi.org/10.1021/acsearthspacechem.0c00294>, 2021.
- 734 Wolfe, G. M., Marvin, M. R., Roberts, S. J., Travis, K. R., and Liao, J.: The framework for 0-D  
735 atmospheric modeling (F0AM) v3. 1, *Geosci. Model Dev.*, 9, 3309-3319,  
736 <https://doi.org/10.5194/gmd-9-3309-2016>, 2016.
- 737 Xu, L., Møller, K. H., Crounse, J. D., Otkjær, R. V., Kjaergaard, H. G., and Wennberg, P. O.:  
738 Unimolecular reactions of peroxy radicals formed in the oxidation of  $\alpha$ -pinene and  $\beta$ -pinene by  
739 hydroxyl radicals, *J. Phys. Chem. A*, 123, 1661-1674, <https://doi.org/10.1021/acs.jpca.8b11726>,  
740 2019.
- 741 Yao, M., Zhao, Y., Hu, M., Huang, D., and Yan, N.: Multiphase reactions between secondary organic  
742 aerosol and sulfur dioxide: kinetics and contributions to sulfate formation and aerosol aging, *Environ.*  
743 *Sci. Technol. Lett.*, <https://doi.org/10.1021/acs.estlett.9b00657>, 2019.
- 744 Zhang, H., Yee, L. D., Lee, B. H., Curtis, M. P., Worton, D. R., Isaacman-VanWertz, G., Offenberg, J. H.,  
745 Lewandowski, M., Kleindienst, T. E., and Beaver, M. R.: Monoterpenes are the largest source of  
746 summertime organic aerosol in the southeastern United States, *Proc. Natl. Acad. Sci. U. S. A.*, 115,  
747 2038-2043, <https://doi.org/10.1073/pnas.1717513115>, 2018.
- 748 Zhao, Y., Thornton, J. A., and Pye, H. O. T.: Quantitative constraints on autoxidation and dimer formation  
749 from direct probing of monoterpene-derived peroxy radical chemistry, *Proc. Natl. Acad. Sci. U. S.*  
750 *A.*, 115, 12142-12147, <https://doi.org/10.1073/pnas.1812147115>, 2018.
- 751 Zhao, Y., Yao, M., Wang, Y., Li, Z., Wang, S., Li, C., and Xiao, H.: Acylperoxy radicals as key  
752 intermediates in the formation of dimeric compounds in  $\alpha$ -pinene secondary organic aerosol, *Environ.*  
753 *Sci. Technol.*, 56, 14249-14261, <https://doi.org/10.1021/acs.est.2c02090>, 2022.
- 754 Zhao, Z., Zhang, W., Alexander, T., Zhang, X., Martin, D. B. C., and Zhang, H.: Isolating alpha-pinene  
755 ozonolysis pathways reveals new insights into peroxy radical chemistry and secondary organic  
756 aerosol formation, *Environ. Sci. Technol.*, 55, 6700-6709, <https://doi.org/10.1021/acs.est.1c02107>,  
757 2021.
- 758